August 2002 • NREL/SR-520-32692

Subcontractor Report

Stable a-Si:H-Based Multijunction Solar Cells with Guidance from Real-Time Optics

Final Report
17 July 1998—16 November 2001

C.R. Wronski, R.W. Collins, J.M. Pearce, R.J. Koval, A.S. Ferlauto, G.M. Ferreira, and C. Chen
Center for Thin Film Devices
Pennsylvania State University
University Park, Pennsylvania

National Renewable Energy Laboratory

1617 Cole Boulevard
Golden, Colorado 80401-3393

NREL is a U.S. Department of Energy Laboratory
Operated by Midwest Research Institute • Battelle • Bechtel

Contract No. DE-AC36-99-GO10337

August 2002 • NREL/SR-520-32692

Stable a-Si:H-Based Multijunction Solar Cells with Guidance from Real-Time Optics

Final Report
17 July 1998—16 November 2001

C.R. Wronski, R.W. Collins, J.M. Pearce, R.J. Koval, A.S. Ferlauto, G.M. Ferreira, and C. Chen
Center for Thin Film Devices
Pennsylvania State University
University Park, Pennsylvania

NREL Technical Monitor: B. von Roedern

Prepared under Subcontract No. XAF-8-17619-22

National Renewable Energy Laboratory

1617 Cole Boulevard
Golden, Colorado 80401-3393

NREL is a U.S. Department of Energy Laboratory
Operated by Midwest Research Institute • Battelle • Bechtel

Contract No. DE-AC36-99-GO10337

NOTICE

Available electronically at http://www.osti.gov/bridge

Available for a processing fee to U.S. Department of Energy
and its contractors, in paper, from:

U.S. Department of Energy
Office of Scientific and Technical Information
P.O. Box 62
Oak Ridge, TN 37831-0062
phone: 865.576.8401
fax: 865.576.5728
email: reports@adonis.osti.gov

Available for sale to the public, in paper, from:

U.S. Department of Commerce
National Technical Information Service
5285 Port Royal Road
Springfield, VA 22161
phone: 800.553.6847
fax: 703.605.6900
email: orders@ntis.fedworld.gov
online ordering: http://www.ntis.gov/ordering.htm

Printed on paper containing at least 50% wastepaper, including 20% postconsumer waste

STABLE a-Si:H BASED MULTIJUNCTION SOLAR CELLS WITH GUIDANCE FROM REAL-TIME OPTICS

Christopher R. Wronski, Robert W. Collins,
Joshua M. Pearce, Randy J. Koval,
Andre S. Ferlauto, Gelio M. Ferreira, and Chi Chen

Center for Thin Film Devices
The Pennsylvania State University
University Park, PA 16802

Phase III Final Technical Status Report
Preparation: November 28, 2001

Subcontract No. XAF-8-17619-22

NREL Technical Monitor: Bolko von Roedern

Table of Contents

Executive Summary

New insights have been obtained into the growth of hydrogenated silicon (Si:H) films via real time spectroscopic ellipsometry (RTSE) measurements. Evolutionary phase diagrams were expanded to include the effects of different deposition conditions, including rf power, pressure, and temperature. Detailed studies of degradation kinetics in thin films and corresponding solar cells have been carried out. Both p-i-n and n-i-p solar cells that incorporate Si:H i-layers deposited with and without H_2-dilution have been studied. For the first time, direct and reliable correlations have been obtained between the light-induced changes in thin film materials and the degradation of the corresponding solar cells.

Previous studies of the evolution of the microstructural and optical properties with thickness in Si:H materials have been extended to include the effects that the optoelectronic properties and microstructure of the material exert on the solar cell characteristics. The influences of the substrate on the microstructure of over-deposited layers have been evaluated by investigating p-i-n solar cell structures incorporating different i-layers, each consisting of sequentially deposited materials whose hydrogen dilution ratios ($R=[H_2]/[SiH_4]$) and thicknesses were changed systematically. The phase transitions indicated by RTSE were further confirmed by these cell studies, and direct correlations have been obtained between the evolution of the Si:H microstructure and cell characteristics. These quantitative results are of critical importance in guiding the design and fabrication of cell structures with improved performance and stability.

A variety of RTSE-deduced phase diagrams for plasma-enhanced chemical vapor deposition (PECVD) of Si:H materials have been established that identify the film thicknesses at which different phase transitions occur during film growth. In such diagrams, the positions of the transitions are plotted in the plane defined by the Si:H bulk layer thickness (d_b) and by the

value of a key deposition parameter. Phase diagrams of d_b vs. R have been developed for Si:H films prepared under a wide range of rf PECVD conditions on both crystalline and R=0 amorphous silicon substrates. The deposition parameters that have been explored include the rf plasma power, substrate temperature, and total gas pressure. These phase diagrams provide insights into the film growth processes that yield a-Si:H with improved electronic quality associated with smooth, stable growth of the surface. The phase diagrams and in particular the transitions of a → a and a → (a + μc) phase boundaries suggest approaches for optimizing Si:H i-layer electronic quality at high deposition rates (> 0.3 nm/s) which will be applied in the fabrication of a-Si:H solar cells.

New insights have been obtained into the stability of a-Si:H thin films and the stability of the corresponding solar cells. The studies of the degradation kinetics for state-of-the-art a-Si:H solar cells and corresponding i layer films have yielded for the first time direct correlations between the fill factors (FFs) and the electron mobility – lifetime products. These correlations have been established for cells with different i-layers as well as for cells with different thicknesses. The studies of SWE via the degradation kinetics under 1 sun illumination for both solar cells and corresponding i-layer films have been extended to include annealing in both the dark and under 1 sun illumination. It has been found that the recovery of the FF and mobility-lifetime product characteristics under 1 sun illumination are similar, as in the case of the degradation kinetics. However, the differences observed when annealing is carried out in the dark versus under 1 sun degraded steady state (DSS) clearly indicate the presence of multiple defects, as has been also found in the recovery from 10 sun DSS[1].

[1] J. M. Pearce, R. J. Koval, X. Niu, S. J. May, R.W. Collins, and C. R. Wronski, "The 'Fast' and 'Slow' Light Induced Defects in Diluted and Undiluted Hydrogenated Amorphous Silicon Solar Cells and Materials", *17th European Photovoltaic Solar Energy Conference Proceedings* Munich (in press).

The detailed studies on both solar cells and the corresponding i-layer materials have also yielded direct correlations between dark J-V and J_{sc}-V_{oc}, thus clearly establishing the superposition principle for both p-i-n and n-i-p cells. These characteristics, including the ability to relate them directly to the i-layer bandgap, the densities of gap states, and the SWE of the i layer, has allowed identification of the elusive contributions of p/i interfaces. This has been achieved by the separation of the recombination in the bulk from that in the p/i interface regions by using cells with different i-layers and protocrystalline p/i interface regions, as well as by using simulations with operational gap state parameters obtained from detailed studies on corresponding i-layer films. The measurements of V_{oc} at different illumination intensities, as well as the dependences of V_{oc} on the bandgap, gap states and SWE of the bulk i-layers, allow the respective limitations on the values and stability of V_{oc} under 1 sun illumination to be established reliably. These results in turn allow meaningful predictions to be made about the ultimate stabilized 1 sun V_{oc}'s that can be achieved with different intrinsic materials.

1. Direct Correlation of SWE in a-Si:H Films with Solar Cell Degradation and Annealing Kinetics

A. Introduction

It has been revealed in the previous Annual Report[2] that the wide range of degradation kinetics in different films under 1 sun illumination cannot be explained by the D^o-dominated model, but by a model that also includes the charged defects. It was also reported that studies with arbitrarily-chosen high intensity tests, although commonly used, are irrelevant in assessing the 1 sun degraded steady states both in thin films and solar cells. This year, the degradation kinetics under 1 sun illumination were studied at different temperatures for both undiluted a-Si:H and diluted protocrystalline Si:H thin film materials, as well as for their corresponding cell structures. The studies were carried out on p-a-SiC:H/ i-a-Si:H/ n-μc-Si:H solar cells with different thicknesses for the i-layers and on the corresponding 1 μm i-layer materials, deposited under conditions reported previously with dilution ratios of hydrogen to silane, $R=[H_2/SiH_4]$, of R=0 and 10. The light I-V's were measured at 25˚C under 1 sun illumination from an Oriel Solar simulator. The measurements of the electron mobility-lifetime ($\mu\tau$) products and α(1.2 eV) were also obtained at 25°C. The latter was determined using dual beam photoconductivity and normalized to transmission and reflection measurement, applying a procedure reported previously[3].

---

[2] STABLE a-Si:H BASED MULTIJUNCTION SOLAR CELLS WITH GUIDANCE FROM REAL-TIME OPTICS For XAF-8-17619-22

[3] L. Jiao, S. Semoushikiana, Y. Lee, and C.R. Wronski, Mater. Res. Soc. Symp. Proc. **467** (1997) 97.

The cells and the films were annealed at 170°C for 4 hours before degradation with 1 sun illumination from either a solar simulator or ELH lamps with IR filters. The temperatures for the degradations were reproducibly obtained within +/-1˚C using a TE Technologies Inc. 1600 temperature controller.

B. Correlation between μτ Degradation Kinetics with Those of FF

The high quality of the R=0 and R=10 intrinsic (i) materials used in this study is indicated by the state-of-the-art fill factors of 0.70-0.71 obtained for i-layers 0.4 μm thick. The kinetics of the R=10 p-i-n cells and their dependence on temperature are similar to those reported last year for the Schottky barrier cell structures whose FF's were dominated by the bulk. The studies have been performed on p-a-SiC:H / i-a-Si:H / n-μc-Si:H solar cells of different intrinsic layer thicknesses with both hydrogen-diluted and undiluted i-layers. These studies have shown that the cell characteristics and light-induced changes are dominated by the bulk i-layers. For the first time, direct correlations have been obtained between the kinetics of light induced changes in films and those in solar cells. It is found that, despite the large temperature dependence of the kinetics between 25 and 100^{o}C, a striking similarity exists between the μτ-products at carrier generation rates of ~10^{19} $cm^{-3}s^{-1}$ and the solar cell fill factors (FF). These direct correlations exist not only for both different thickness cells but also at different temperatures. This is illustrated in Fig. 1, which depicts results for a cell having a 7000Å R=10 i-layer upon degradation under 1 sun illumination at 25°C and 75°C. These results clearly show a linear relationship between μτ and FF. In addition to such studies of degradation kinetics with different i layer materials and thicknesses, annealing kinetics have also been investigated both in the dark as well as under 1 sun illumination.

The annealing kinetics from the 10-sun degraded steady state, measured in the dark and under 1 sun illumination, were studied for both protocrystalline thin film materials and their corresponding cell structures. Strong similarities are found in the annealing kinetics for cells and films as seen in Fig. 2. Here, results are shown depicting the recoveries at 50°C for a 700 nm thick p-i-n solar cell and for the μτ-products of the corresponding i layer film after degradation to a 10-sun DSS at 50˚C. These results illustrate not only the kinetics associated with "fast" and "slow" states discussed previously but also clearly reveal the contributions of "light annealing" in both the film and cell[4].

Contributions of the "fast" and "slow" states could also be identified in the degradation kinetics of μτ and FF under 1 sun illumination and direct correlations are found between their respective changes to the DSS. However, there are no such direct correlations between the μτ and FF with the densities of gap states as characterized by the magnitude of subgap absorption (α(E)) at 1.2eV as measured by DBP. The approaches taken in these as well as earlier studies have been cognizant of the importance of the non-D˚ gap states in determining μτ, which are not directly detected from α(1.2eV) and their contribution to both the kinetics of light induced changes as well as their DSS[5].

C. Correlation between Dark J-V Characteristics with Those of Subgap Absorption

Although there are no direct correlations between the kinetics of degradation or annealing for the subgap absorption values, α(1.2 eV), and for either the FF or the μτ-products, there is in fact a correlation between the subgap absorption and the dark J-V characteristics. This similarity

[4] L. Yang, L. Chen, and A. Catalano, Appl. Phys. Lett. **59**, (1991) 840.
[5] J. Pearce, X. Niu, R. Koval, G. Ganguly, D. Carlson, R.W. Collins, C.R. Wronski, *Mat. Res. Soc. Proc.*, **664**, A12.3, 2001.

between the subgap absorption and dark J_D-V is illustrated in Fig. 3, which depicts results under 1 sun prolonged illumination at 25°C for a p-i-n solar cell with an R=10 i-layer (inverted triangles). Figure 3 compares the normalized degradation, in percent, for the $\alpha(E)$ values at 1.2 eV in the i-layer material and the corresponding bulk-dominated dark current at 0.4 V forward bias in the 0.4 μm R=10 p-i-n cell. The value of 0.4 V is chosen because it represents a bias in the exponential region of the dark characteristics, associated with the generation-recombination through defects at or near the mid-gap. The energy of 1.2 eV is adopted here because subgap absorption at this value is generally used to represent the density of dangling bond states (D°). It has been shown that linear relationships exist between the values of α(1.2 eV) and the densities of D° states as measured by ESR; however, the slopes can be different for different materials, thus showing that there is no single conversion factor between α(1.2 eV) and the densities of D°. As seen in Fig. 3 the rate of defect creation in the midgap region is proportional to the increase in dark current of the exponential J_D-V characteristics. The results here show clearly that, in properly-fabricated high-quality p-i-n cells, the dark J_D-V characteristics in the exponential region and J_0 are bulk dominated and can be directly correlated with both the intrinsic and light induced states. This conclusion has been utilized in obtaining further insights into cell characteristics under illumination, for example, the determination of the bulk limitations on the open circuit voltage (discussed in Section 3).

2. Higher Rate Growth of a-Si:H i-Layers

A. Introduction

Deposition phase diagrams first developed at Penn State have proven useful for describing the growth processes of hydrogenated silicon (Si:H) thin films prepared by plasma-enhanced chemical vapor deposition (PECVD). In the simplest phase diagrams, the bulk layer thickness d_b at which the amorphous-to-(mixed-phase-microcrystalline) transition occurs is plotted as a continuous function of one of the deposition variables. The variable of greatest interest is the hydrogen-to-silane gas flow ratio $R=[H_2]/[SiH_4]$, which is used most widely for phase control in Si:H PECVD. Diagrams with other variables that control the microstructure and phase of the materials, such as the substrate temperature or total gas pressure, have also been developed.

More recently so-called "extended" phase diagrams have been established, incorporating multiple transitions that characterize the microstructural evolution of Si:H films. The extended diagrams include:

(i) surface roughening transitions in which the Si:H film is amorphous on both sides of the transition [a→a];

(ii) surface roughening transitions from an amorphous phase to a mixed (amorphous + microcrystalline) phase [a→(a+μc)]; and

(iii) surface smoothening transitions from the mixed (amorphous + microcrystalline) phase to a single (coalesced) microcrystalline phase [(a+μc)→μc].

The extended diagrams are valuable in providing insights into Si:H film growth mechanisms; in addition, such diagrams can guide materials and solar cell fabrication. For example, optimum a-Si:H based i-layers for p-i-n solar cells are prepared at the lowest possible rf

plasma power within a stable-surface regime of amorphous film growth defined by a narrow window in R. At higher R values for the desired i-layer thickness the a→(a+μc) transition occurs, whereas at lower R values the a→a transition occurs. It is found that the narrow window closes and the stable-surface regime disappears when the rf power is elevated above its minimum in attempts to increase the deposition rate of a-Si:H above 0.5 Å/s to > 3 Å/s. This phase diagram behavior has been correlated with significant reductions in overall device performance, and studies have focused on attempts to understand the growth processes under conditions that result in higher deposition rates.

It is generally recognized that the most effective approaches for increasing the Si:H deposition rates in rf PECVD do not simply involve increasing the plasma power. In fact, silane partial pressure, substrate temperature, and/or the H_2-dilution ratio must also be varied in any attempts to optimize the electronic quality at higher rates. Thus, our phase diagram studies have been expanded to explore, not only the effects of increased rf power, but also the role of the substrate temperature and the total gas pressure.

B. Experimental Details: Depositions

The Si:H films were deposited in a single chamber reactor having an rf diode parallel-plate electrode configuration with an electrode spacing of 1.9 cm. The substrate was native oxide-covered crystalline Si (c-Si). The phase diagrams presented in this study were derived from a series of depositions using different H_2-dilution ratios (R). Different fixed values of the rf plasma power (P), substrate temperature (T_s), and total pressure (p_{tot}) were investigated in these studies. The relevant deposition conditions, together with the corresponding range of deposition rates, are summarized in Table I.

C. Experimental Details: Real Time Optics

RTSE was performed during each deposition using a rotating-compensator multichannel ellipsometer. This instrument provides the Stokes vector of the light beam reflected from the growing sample over the photon energy range from 1.5 to 4.7 eV, with full spectra acquisition and repetition times of 1 s. The parameters that define the Stokes vector include the tilt and ellipticity angles of the polarization ellipse, the reflected-to-incident irradiance ratio, and the polarization degree. These parameters can be established from 8 photodiode array detector readouts over the 50 ms optical cycle of the rotating MgF_2 compensator. The experimental data sets are analyzed applying a two-layer model, including surface roughness and bulk layers with thicknesses of d_s and d_b, respectively. The optical properties of the roughness layer are estimated from the Bruggeman effective medium approximation as a 0.50/0.50 volume fraction mixture of (bulk material)/voids.

D. Overview of the Microstructural Features

In this section, the various signatures in the time evolution $d_s(t)$ are described, along with their interpretations in terms of the microstructural evolution and phase transitions. Initially the focus is on results such as in Figs. 4 and 5, where the surface roughness layer thickness d_s is plotted versus the bulk layer thickness d_b throughout the growth of Si:H films from d_b=10 Å to d_b~5000 Å. The depositions of Figs. 4 and 5 were performed using two H_2-dilution ratios R of (10, 40) and two rf power levels P of (0.08, 0.8) W/cm^2.

(I) *Coalescence of initial amorphous nuclei*. Coalescence of nucleation-induced microstructure is observed as a smoothening effect during a-Si:H film growth in the first ~100 Å of bulk layer thickness. Such an effect can be observed for both R=10 depositions in Fig. 4 and for the (R=40, P=0.8 W/cm^2) deposition of Fig. 5. For these three depositions, the films nucleate

on the c-Si substrate as a-Si:H clusters. The magnitude of this smoothening effect can be characterized by $\Delta d_s = d_s(2.5\ \text{Å}) - d_s(100\ \text{Å})$ [where $d_s(x)$ is the value of d_s when $d_b=x$]. The a-Si:H films with the largest Δd_s exhibit the best electronic performance for applications as i-layers in solar cells -- as long as the films remain amorphous throughout the deposition.

(II) *Coalescence of initial microcrystalline nuclei.* An even larger smoothening effect can be observed upon structural coalescence of clusters that nucleate directly on the substrate as microcrystalline silicon (μc-Si:H). This larger effect can be observed for the (R=40, P=0.08 W/cm^2) deposition of Fig. 5. In this case, the much larger d_s value at the onset of bulk layer growth is due to a lower initial nucleation density compared to that of the a-Si:H films. The mechanisms that control amorphous and microcrystalline cluster coalescence are believed to be different (surface diffusion vs. competitive space filling, respectively).

(III) *Stable surface growth.* Under a narrowly-defined set of deposition conditions (specifically, in Fig. 4 for R=10 and P=0.08 W/cm^2), the a-Si:H surface remains smooth and stable with < 1 Å change in the roughness layer thickness from the end of coalescence through thick film growth, e.g., from 100 to 4000 Å in the example of Fig. 4. When the stable surface regime is present, it is found to occur at an R value just prior to the a→(a+μc) transition. Under these conditions, highest performance and stability materials for solar cells are obtained.

(IV) *Amorphous roughening transition.* If one starts with the stable-surface deposition conditions, for example (R=10, P=0.08 W/cm^2) in Fig. 4, and gradually decreases R or increases P, then a roughening transition is detected that gradually shifts to lower d_b. The growing film is amorphous on both sides of this transition, and the associated surface microstructural changes are correlated with reductions in the performance and stability of such films as i-layers in solar cells.

A shift in the a→a roughening transition to lower d_b appears to reflect a reduction in the surface diffusion length of the adsorbed radicals that form the film.

(V) *Amorphous–to–mixed-phase-microcrystalline) (a+μc) transition.* At moderate to high values of R, for example R=40 and P=0.8 W/cm^2 in Fig. 5, a different type of roughening transition is observed in which crystallites nucleate from the growing amorphous phase. Because the nucleation density is usually low, the crystalline protrusions generate a surface roughness layer that increases rapidly in thickness with increasing d_b. For the example in Fig. 5, this transition occurs at d_b=170 Å.

(VI) *(Mixed-phase)–to–(single-phase) microcrystalline transition.* For thin films that have already undergone an a→(a+μc) transition, a second transition is possible that occurs at even greater bulk layer thicknesses. In this transition, the crystalline protrusions that extend above the surface make contact, leading to a coalescence process with continued film growth. This process is manifested in the data as a transition from surface roughening to smoothening. Once the crystallites have coalesced to cover the growing film surface completely, single-phase μc-Si:H growth proceeds with a resumption of surface roughening. An example of such a transition is evident for the film of Fig. 5 with (R=40, P=0.8 W/cm^2), at d_b=850 Å.

E. Results and Discussion

i. Effect of Plasma Power at Low Temperature

Figure 4 provides a comparison of the surface roughness evolution for the deposition series **A** and **B,** i.e., for low and high rf power levels, respectively, at fixed T=200°C and R=10. First, it is evident that the surface smoothening magnitude Δd_S during initial coalescence [signature (I)

above] decreases with increasing rf plasma power. The Δd_s values are 7.5 Å for P=0.08 W/cm^2 (rate: 0.5 Å/s) and 5 Å for 0.8 W/cm^2 (rate: 3.5 Å/s). Such behavior is observed independent of R, throughout the regime in which a-Si:H nucleates. Second, it is evident that the stable-surface condition [signature (III)] obtained at P=0.08 W/cm^2 is lost with the increase in power. In fact, for the deposition with P=0.8 W/cm^2, an a$\rightarrow$a roughening transition [signature (IV)] is evident in Fig. 4 at d_b=500 Å (arrow). Stepwise increases in the power above P=0.08 W/cm^2 reveal that the amorphous roughening transition appears at the highest d_b of 4000 Å and then shifts monotonically to lower d_b with increasing P.

The reduction in Δd_s and the shift in the a$\rightarrow$a roughening transition to lower d_b with increasing rf power can both be attributed to a reduction in the diffusion length of adsorbed radicals on the a-Si:H surface. This may be explained by (i) enhanced ion bombardment of the surface that generates reactive sites for immobilization of the radicals; (ii) enhanced generation of plasma species with lower surface diffusion length, either SiH_n (n<3) owing to SiH_4 depletion in the plasma, or higher silanes Si_mH_n (m>1) owing to radical-radical reactions in the plasma; or (iii) reduced concentration of beneficial H radicals relative to reactive SiH_n radicals reaching the surface at the higher rf plasma power.

Figure 5 depicts a comparison of the surface roughness evolution for deposition series **A** and **B**, but now with T=200°C and R=40. Here, it is evident that the immediate μc-Si:H nucleation and subsequent coalescence [signature (II)] that occurs on the c-Si substrate at P=0.08 W/cm^2 (rate: 0.2 Å/s) is suppressed with the increase in power to 0.8 W/cm^2 (rate: 2.0 Å/s). At the higher rf power, an amorphous phase evolves first from the substrate [signature (I)], followed by an a$\rightarrow$(a+μc) transition at d_b=170 Å [signature (V)], and an (a+μc)$\rightarrow$μc transition at d_b=850

Å [signature (VI)]. In spite of the differences in the structural evolution, the final single-phase μc-Si:H films of series **A** and **B** exhibit similar roughness layer thicknesses at the end of deposition.

The changes in the nucleation behavior as the rf power is increased are likely to be explained by a shift in the PECVD process from one in which atomic H etching of initial nuclei is dominant (at low power) to one in which amorphous film growth is promoted with insufficient etching to generate microcrystallites on the substrate (at high power). Such behavior supports explanation (iii) of the previous paragraph.

The results from deposition series **A** and **B**, provide the two overlapping phase diagrams of Fig. 6. In this figure, the boundaries are plotted corresponding to the a→a transitions [broken lines, signature (IV)] and the a→(a+μc) transitions [solid lines, signature (V)] for series **A** (circles) and **B** (squares). The effects of power on the transition lines are clear. First, with the increase in P, the a→a transition is shifted to lower d_b by at least an order of magnitude. Second, at moderately high R ($R \geq 20$), the a→(a+μc) transition is shifted to higher d_b, apparently owing to the suppression of H etching (e.g., for R=40) or owing to the higher rate growth kinetics at high plasma power (e.g., for R=20). Finally, a reversal of this second effect appears to occur at intermediate R (R=15). For this latter film, the smooth surface obtained at low power may suppress microcrystallite nucleation from the amorphous phase, whereas the tendency toward roughening at higher power due to the a→a transition may promote nucleation. It is important to note that the window for smooth, stable-surface deposition, observed near (R=10, P=0.08 W/cm^2), just prior to the onset of the a→(a+μc) transition, closes with the increase in power. This is consistent with the observed reduction in solar cell performance

observed when the power is increased even moderately above the optimum (lowest possible) value.

ii. Effect of Temperature at High Plasma Power

Next, the effect of substrate temperature (T) at the elevated plasma power level is explored. Figure 7 shows a comparison of results from deposition series **B** and **C**, i.e., the effect of an increase in T from 200°C to 260°C, for the fixed values (R=0, P=0.8 W/cm^2). Although the a-Si:H nucleation densities are similar for the two temperatures, an enhancement in the smoothening during coalescence and a shift in the amorphous roughening transition to larger d_b are both observed at the higher temperature. These results are consistent with an expected increase in the precursor surface diffusion length at the higher substrate temperature. Figure 8 shows the corresponding results for R=10. In this case, the elevated temperature has two primary effects, namely, an increase in the magnitude and rate of surface smoothening during coalescence and the appearance of an a$\rightarrow$(a+μc) transition near d_b=700 Å (arrow). The latter transition is determined from the roughness evolution, as well as from the dielectric function.

The results from series **B** and **C** are incorporated into the phase diagrams superimposed in Fig. 9. It is clear from Fig. 9 that the increase in T leads to a modest reversal of the effects of high power to the extent that the amorphous roughening transition now shifts back to higher d_b. However, the stable-surface condition cannot be regained owing to the shift in the a$\rightarrow$(a+μc) transition to lower R. This behavior suggests that the improvements in solar cell performance that may have been expected by increasing T for i-layers prepared at higher power, are in fact limited owing to the need to reduce R simultaneously in order to avoid the a$\rightarrow$(a+μc) transition.

iii. Effect of Pressure at Elevated Plasma Power

Next, the effect of pressure (p_{tot}) at the elevated plasma power level is described. Figure 10 shows a comparison of results from deposition series **B** and **D**, i.e., the effect of an increase in pressure from p_{tot}=0.4 to 4 Torr. The plasma power in the series **D** deposition was lower (P=0.34 W/cm^2) and the H_2 dilution ratio was higher (R=60), in order to achieve comparable deposition rates (0.35 and 0.34 nm/s, respectively) and similar positions just on the amorphous side of the a→(a+μc) boundary. First, Fig. 10 shows that the density of a-Si:H nuclei is lower at the higher pressure, possibly suggesting that the density of bombardment-induced defects sites for nucleation on the substrate is lower as well. Second, a strong enhancement in the smoothening during coalescence and a shift in the amorphous roughening transition to larger d_b are both observed at the higher pressure. These second observations are both consistent with an increase in the precursor surface diffusion length at the higher pressure. This may occur due to the reduction in ion bombardment or to an improvement in the plasma chemistry. Perhaps the higher H_2-dilution balances the flux of atomic H and SiH_n film-forming radicals reaching the film surface.

In Fig. 11, the phase transitions for the Si:H films of series **B** and **D** are compared. The increase in pressure leads to a substantial change in the phase diagram, in particular, a significant shift of the a→(a+μc) transition to much higher R. As a result, there exists a broad range of R (20–60) wherein the amorphous roughening transition occurs at relatively large thicknesses (d_b > 100 nm), indicating films of improved electronic quality for series **D** compared with those of series **B**.

iv. Effect of Substrate at High Plasma Power

Next the effect of substrate nature on the phase diagrams will be explored, focusing on the 200°C Si:H depositions at the two rf power levels. Figure 12 shows the final results of the phase diagrams for Si:H film growth at the lower rf power of 0.08 W/cm^2 on native-oxide covered c-Si wafers and on R=0 a-Si:H films, as deduced from roughness evolution data such as those presented in Figs. 4-5 and 7-8. Figure 13 shows the corresponding diagrams for Si:H film growth on the two substrates at the elevated rf power of 0.8 W/cm^2, for comparison. With the use of the R=0 a-Si:H substrate, it is clear that the a$\rightarrow$(a+μc) transition is shifted to higher bulk layer thicknesses d_b in comparison to the transition observed for c-Si wafer substrates. Thus, the a-Si:H substrate is effective at suppressing crystallite development for all explored conditions of R and P. This suppression is likely to have at least two causes. First, at moderately high R (R≥20), a low density of nuclei may develop directly on the c-Si wafer substrate even below the detected a$\rightarrow$(a+μc) transition. Any such direct nucleation is likely to be suppressed by the R=0 a-Si:H substrate. Alternatively, Si:H films grown on c-Si wafer substrates may exhibit a higher degree of order than those grown on R=0 a-Si:H substrates. The higher ordering may increase the probability of microcrystallite nucleation from the amorphous phase. Finally, if the a$\rightarrow$(a+μc) transition is driven ultimately by the build-up of stress in the network, then the a-Si:H substrate may be more effective than the c-Si substrate in suppressing this build-up. If the stress is generated by non-bonded trapped hydrogen, then the a-Si:H substrate may be more effective as a sink for this hydrogen.

F. Overview and General Discussion on High Rate Growth

Figure 14 depicts the evolution of the surface roughness layer thickness vs. the bulk layer thickness for selected a-Si:H films of each series **A-D** deposited under nominally "optimum conditions", defined as the maximum H_2-dilution possible without crossing the a→μc transition for a 3000 Å a-Si:H film. It should be emphasized that for all films the deposition rates are higher than 3 Å/s, except for the R=10 film of series **A** (r = 0.5 Å/s). In fact, the result for this latter film demonstrates roughness evolution characterized by smooth, stable surface after nuclei coalescence and throughout the growth of a 3000 Å a-Si:H layer. This behavior correlates with the highest observed solar cell performance in initial and fully light-soaked states.

Figures 4-6 and 14 suggest that increasing the plasma power while keeping other parameters fixed is detrimental to the film quality. At low H_2-dilution (R≤10) where the films are amorphous throughout growth, an observed suppression of the surface smoothening upon initial nuclei coalescence and the significant reduction in the a→a roughness transition thickness evident in Fig. 14 with the increase in plasma power both indicate a reduction in the surface diffusion length of the absorbed radicals (or alternatively the reactive sites for radical attachment). The reduction in surface diffusion length at high plasma power can be attributed to (i) enhanced generation of plasma species with lower surface mobility, either reactive SiH_n (n<3) or higher silanes Si_mH_n (m>1); (ii) enhanced ion bombardment of the surface that generates a higher density of reactive sites for radical attachment; and/or (iii) reduced concentration of beneficial H radicals relative to SiH_n (n≤3) radicals reaching the surface. The latter effect may also explain the increase in the a→(a+μc) transition thickness with increasing power for higher R (R=20-40), since it is believed that atomic H promotes relaxation of the Si network, thus favoring nucleation of Si microcrystals in the top few monolayers. It is clear in

Fig. 4 that the narrow window for smooth, stable-surface deposition, observed in series **A** near R=10 just prior to the onset of the a→(a+μc) transition closes as the rf plasma power is increased. This is consistent with the observed reduction in solar cell performance when the power is increased even moderately above the optimum (lowest possible) value.

An obvious approach to counterbalance the detrimental effects of an increase in rf plasma power is to increase the substrate temperature, thereby enhancing the mobility of the adsorbed surface radicals. The results of Figs. 7-9 and 14 indicate that a modest increase in T_s does indeed exert weakly beneficial effect within the amorphous regime, i.e., an increase in the a→a transition thickness. However, the optimum stable surface window observed at the low power and R=10 is not recovered at the higher temperature for any R. This fact is illustrated through the comparison of the roughness evolution in Fig. 14 for the nominally-optimized film of series **C** with those of series **A** and **B**. This observation suggests that within the low-temperature range (T_s<300°C), plasma chemistry dominates the film growth processes. It is possible that a higher range of T_s may provide more pronounced beneficial effects on the film growth at high rates, however such a range would be of limited value for the a-Si:H i-layers of p-i-n solar cells.

Finally, we consider the effect of total gas pressure as depicted in Figs. 10, 11, and 14. For R=10, p_{tot} = 4 Torr, and P=0.3 W/cm^2, the deposition rate is significantly higher (7.9 Å/s) than for R=10, p_{tot}=0.3 Torr, and P=0.8 W/cm^2 (r = 3.5 Å/s), reflecting an increased probability of the dissociation reactions that produce SiH_n (n≤3) radicals. The formation of higher silanes inherent in high-pressure deposition, however, leads to a decrease in the a→a transition thickness for R=10. By increasing R above 10, the additional H_2 in the plasma may inhibit formation of the detrimental higher silanes, thus accounting for the significant increase in the a→a transition thickness. The shift of the a→(a+μc) transition to much larger R (R>60) can be explained by the

increased probability of the reaction $SiH_4 + H \rightarrow SiH_3 + H_2$, that reduces the ratio of atomic H to SiH_n ($n \leq 3$) radicals reaching the surface. Thus, the results of Fig. 14 suggests that the H_2-dilution can be used effectively at high pressures to balance the flux of atomic H and SiH_n film-forming radicals reaching the film surface, yielding a-Si:H films with surfaces that are smooth and stable throughout a considerable range of bulk film thickness (d_b>1000 Å). Another possibly relevant factor in maintaining smooth, stable surfaces is the reduction in ion bombardment. Ion bombardment is expected to exert detrimental effects at higher powers by increasing the density of reactive sites at the surface and reducing the surface diffusion length of adsorbed radicals.

G. Final Remarks

Deposition phase diagrams plotted in the plane of the bulk layer thickness and the H_2-dilution ratio for Si:H films prepared by rf PECVD have illustrated the effects of rf plasma power, substrate temperature, and total gas pressure on Si:H film growth processes. These diagrams show that an increase in the rf power is detrimental to a-Si:H electronic quality and that a modest increase in T_s does not lead to a significant recovery of film quality. On the other hand, dramatic changes in the phase diagrams as the total pressure is increased suggest that this parameter can be used effectively for the optimization of Si:H film deposition at higher rates. Finally, the phase diagrams and in particular the positions of the a→a and a→(a+μc) phase boundaries, suggest approaches for optimizing Si:H i-layer electronic quality at the higher rates.

3. Optimization of Solar Cells

A. Phase Transition Effects on Device Performance

The optimization of a-Si:H based solar cells incorporating "hydrogen-diluted" i-layer materials is severely complicated by the recently-established evolution of the microstructural and optical properties with thickness for these materials, as well as the strong effect of the substrate on the microstructure of the over-deposited materials (as discussed in Section 2 and previous reports). This complexity is exacerbated for cell structures optimized using the previously-developed two-step i-layer process in which the p/i interface region is deposited with a higher hydrogen dilution ratio R ($R \equiv [H_2]/[SiH_4]$) than that used for the bulk i-layer. The inhomogeneity and anisotropic nature of these evolving i-layer materials also give rise to difficulties in correlating the properties of thin films with device characteristics due to the inherent differences between transverse carrier transport in the cell configuration and in-plane transport in the standard coplanar configuration. During this year, correlations were established between electronic characteristics of cell structures having different i-layer thicknesses / hydrogen dilution ratios and real-time optical characteristics of i-layers prepared under the same conditions and on similar substrates. The design of the cell structures as guided by real-time optics has allowed meaningful correlations to be made between the microstructure of the i-layer material and the cell characteristics.

To assess the effects of transitions from the amorphous phase to the mixed (amorphous + micro-crystalline) phase, cell structures incorporating such transitions at different depths in the i-layer from the p-contact have been investigated and compared to a standard cell structure. Experimental results have been obtained that clearly demonstrate changes in the mobility gap,

E_μ, of the materials as their microstructure evolves with thickness, further supporting the important effect of the hydrogen dilution ratio R ($R \equiv [H_2]/[SiH_4]$) and substrate on the transition between the a-Si:H and (a+μc)-Si:H phases.

Previous reports have focused on the effects of the thickness-dependent a→(a+μc) phase transitions in Si:H i-layers on the performance and stability of a-Si:H based solar cells[6]. Figure 15 depicts the initial fill factors (FF) of cells prepared with i-layer thicknesses from 1100 Å to 1 μm, a range over which such transitions occur. Here, the i-layers are prepared using $0 \leq R \leq 20$; otherwise, identical deposition conditions are used overall. At a thickness of 1100 Å, the initial FFs of all cells are virtually the same, irrespective of R. For R=0, where no phase transition occurs over the entire i-layer thickness range, the FF decreases as expected in a manner closely matching that of the numerical AMPS simulations, the latter obtained assuming a uniform homogeneous i-layer. These simulations used operational parameters for both dangling bonds and charged defects, as obtained in previously reported studies. However, for the cells prepared with H_2-dilution of i-layers, thickness-dependent deviations from the R=0 FFs are clearly discernible. These can be attributed to the phase transitions in the bulk layers as indicated by the phase diagram developed by RTSE for Si:H film deposition on amorphous film surfaces, as discussed above. Importantly, the RTSE results have shown that the phase transition in the Si:H materials is not abrupt, but passes through an amorphous + microcrystalline (a+μc) mixed-phase region, in which the microcrystallites embedded in the amorphous matrix increase in in-plane scale with increasing thickness.

[6] STABLE a-Si:H BASED MULTIJUNCTION SOLAR CELLS WITH GUIDANCE FROM REAL-TIME OPTICS For XAF-8-17619-22

Insights into the transitions, as well as their effect on solar cell characteristics, were obtained from studies carried out on different cell structures. Three examples of such structures are discussed here. Cell 'A' is the optimized protocrystalline structure that incorporates a 200Å R=40 p/i interface region and an R=10 bulk region. Such a solar cell has a relatively homogeneous i-layer. Cell 'B' is deposited with a one-step R=20 i-layer. The phase diagram shown in previous reports has demonstrated that the a→(a+μc) transition in the R=20 i-layer, if deposited on an amorphous film substrate (as is present in cell 'B'), occurs after an accumulated film thickness of approximately 1000 Å. In cell 'C', a 400 Å R=40 p/i interface (which has traversed the a→(a+μc) boundary) was followed by an R=20 bulk i-layer region. Ellipsometry studies have also demonstrated that the growth of the same R=20 layer on an R=40 layer that has traversed the a→(a+μc) phase boundary proceeds in the microcrystalline phase. As a result, the i-layer of cell 'C' is fully microcrystalline with the exception of the initial 400 Å. In fact, the first 200 Å of the i-layer of cell 'C' is amorphous whereas the next 200 Å is mixed-phase Si:H [(a+μc)-Si:H] and the remainder of the i-layer (3600Å) is single-phase μc-Si:H.

The experimental J-V characteristics at room temperature for cells A, B, and C are shown in Fig. 16 for 1 sun illumination and in Fig. 17 for the dark. It can be seen in Fig. 16 that the FF and V_{oc} are the highest for cell A since the thickness and R values in the two step i-layer are chosen in order to maintain protocrystallinity [i.e., Si:H deposition just on the amorphous side of the a→(a+μc) phase boundary]. The cell performance becomes progressively worse for cells B and C, as the position of the phase boundary in the i-layer approaches the p-contact (indicated by the direction of the arrows).

This drop in cell performance is a result of the presence of a narrow gap material in the i-layer of cells B and C, as reflected in the dark J-V characteristics shown in Fig. 17. In p-i-n

structures most of the carrier recombination occurs in a narrow region, approximately halfway between the p- and n- contacts at low forward bias. This region extends toward both contacts at higher forward bias, as can be seen in Fig. 18. This figure shows the bias-dependence and spatial non-uniformity of the carrier recombination rates in a p-i-n cell with a homogeneous amorphous i-layer as obtained from AMPS simulations using established operational parameters. Inflection points in the dark J-V characteristics observed in Fig. 17 can thus be explained by the large contribution of the narrow gap material to the recombination currents at low forward bias. The eventual merging of the currents at higher forward bias in cells B and C with that of cell A in Fig. 17 is due to a shift of the recombination from the bulk i-layer to the vicinity of the contact layer regions (which are similar for all three cells). The forward bias voltage at which the dark current of cell C merges with that of cell A is larger than the corresponding bias for cell B. This behavior occurs because the phase boundary in cell C is closer to the p-layer so that the carrier recombination in the narrow gap material dominates over a larger voltage range. The large decreases of the FF in cells B and C are a direct consequence of the phase transitions. Specifically, the higher photogenerated carrier densities in the narrow gap μc-Si:H portion of the i-layer lead to a collapse of the electric field in that region in order to maintain current continuity across the entire i-layer. As a consequence, most of the voltage drop must occur across the wide gap amorphous region. The weaker average field across the i-layer results in the anomalous inflection point in the light J-V characteristics as seen in Fig. 16. This effect becomes more pronounced as the phase transition approaches the p-contact.

The increase in carrier recombination in the microcrystalline portion of the i-layer in cells B and C, inferred from the magnitude of the dark currents under small forward bias, is attributed primarily to changes in the mobility gap. Such behavior is consistent with that predicted from

the evolutionary phase diagram, as the material evolves from a wide gap amorphous phase to a narrow gap microcrystalline phase. Evidence for the change in the mobility gap that occurs as the Si:H material evolves across the phase transition is obtained from the temperature dependence of the reverse saturation current (J_o), as discussed in the last report. This is evident from Fig. 19 wherein plots of J_o/T^3 versus $(2kT)^{-1}$ are shown for cells A and C. The value of 1.88 eV obtained for cell A is in agreement with the mobility gap measured for the same i-layer material via internal photoemission. Furthermore, the decrease in activation energies from this value to 1.15 eV for cell C confirms the ellipsometry results indicating that such an i-layer is predominantly microcrystalline. These results confirm the positions of the phase boundaries in different i-layer materials prepared with different R values and on different substrates and, in addition, reveal the effects of these boundaries on the cell characteristics. The insights obtained here are of critical importance in the design and fabrication of cell structures with improved performance and stability.

B. Limitations on the Open Circuit Voltage in a-Si:H Solar Cells

Despite the progress in understanding the limitations on the open circuit voltage (V_{oc}) of a-Si:H based solar cells, there are still many unanswered questions about the mechanisms responsible for these limitations[7]. It is generally accepted that, in addition to the generation-recombination in the i layer, the main contributing factors to V_{oc} are the TCO/p and i/n contacts as well as the p/i interface region. Of these factors, the n contact and i/n region have been found to exert the smallest effect on our cells, as indicated by the fact that n+ a-Si:H and μc-Si:H contacts give the same V_{oc} and FF.

[7] J. Pearce, R. Koval, A. Ferlauto, R. W. Collins, C.R. Wronski, J. Yang, and S. Guha, *Appl. Phys. Lett*. **77**, 3093 (2000).

Effects of both the TCO/p contact and the p-layer itself have been investigated, but it has been difficult to separate the two. In particular, it has been difficult to identify and characterize the exact nature of the TCO/p contacts, although distinct differences are found between SnO_2 and ZnO in both V_{oc} and FF. These factors have also been explored by changing the nature of the a-SiC:H p layers while examining systematically the dependence of V_{oc} on the thickness and doping level of the p-layer. The extensive efforts undertaken to improve V_{oc} by applying improved p/i interface layers have been successful. However, in spite of this progress, the contributions of the p/i regions and the bulk i-layer to the limitations on V_{oc} have not been identified carefully nor quantified reliably.

This year, detailed studies were continued in which the high quality protocrystalline Si:H intrinsic layers were unchanged in the structure, and the p/i interface regions and p layers were systematically varied. This was carried out by fabricating p-i-n solar cells with 20 nm regions adjacent to the p a-SiC:H having different H_2 dilution levels, as well as fabricating n-i-p cell structures comparing p-type a-SiC:H and μc-Si:H. Because of the high quality of the intrinsic material, even "good" p/i interface regions have a significant effect on both the (dark current)-voltage (J_D-V) and V_{oc} characteristics. The studies carried out here have allowed the contributions to the V_{oc} of different p/i interface regions as well as the bulk regions to be identified and quantified for cell structures exhibiting both high V_{oc} values and high fill factors (0.72 for 400 nm i layers).

The solar cells were fabricated by RF plasma enhanced chemical vapor deposition applying a recipe for intrinsic protocrystalline Si:H that uses SiH_4 diluted in hydrogen with a dilution ratio of R = 10 (under conditions described previously). The p-i-n structures consisted of specular SnO_2/ p a-SiC:H (25 nm)/ i a-Si:H (400 nm)/ n μc-Si:H (25 nm)/ Cr, and the n-i-p

structures were specular glass/ Cr/ n a-Si:H (25 nm)/ i a-Si:H (400 nm)/ p Si:H/ ITO. In the solar cells, the 20 nm p/i interface region was systematically improved by increasing the R value from 10 to 40. To minimize possible contributions of shunts to the dark J-V's at low forward bias, small areas (0.02 cm^2) were defined by reactive ion etching of the n-type μc-Si:H layers. The J_D-V and J_{sc}-V_{oc} characteristics were measured at 25˚C, with the latter being obtained under illumination between ~10^{-7} and ~50 suns. Results were obtained on cells in the annealed state (4 hours at 170˚C) as well as in the 1 sun degraded steady state (DSS) obtained after 100 hours of illumination at 25°C.

AMPS simulation code was used to gain insights into the physical nature of the device characteristics using operational parameters obtained from studies on thin films using SAM. In the past it has been difficult to model the contacts reliably because of the absence of reliable parameters for the densities of defects in both the a-Si:H and a-SiC:H as well as for the band offsets between a-SiC:H and a-Si:H. As a result, ad-hoc assumptions and simplifications have been made. In the AMPS simulations carried out here, the same p-type a-SiC:H – TCO contact represented by a flat band 'dead' p layer was used. The degraded steady states were modeled by increasing the densities of defects in accordance with experimental results obtained for ESR spin densities and subgap absorption.

The actual nature of the p/i interface is difficult to classify. It can be defined as the monolayer between the p and i-layers and, in addition, as the extended region into the i-layer. Very large effects on V_{oc} have been found for p/i interface regions a few hundred Ångstroms thick in the form of highly diluted a-Si:H layers, which yield significant systematic improvements in V_{oc}. In these p/i regions, the large carrier recombination that limits the 1 sun V_{oc} in cells is significantly reduced, but instability is still exhibited due to SWE in the bulk.

In solar cells with high-quality interfaces, the carrier transport and recombination in the dark and under illumination can be controlled by the bulk of the i-layer over extended regions of forward bias. However, in both cases for a sufficiently high forward bias, the recombination in the p/i interface regions begins to play a dominant role. Figure 20 shows an AMPS simulation of the recombination rates under different illumination levels for a p-i-n solar cell with a 0.4 μm R=10 i-layer, as measured in the DSS. In this simulation there are no additional p/i interface states, i.e., the material is identical to the bulk all the way to the p-layer. The arrow indicates an increase in illumination intensity from 0.0001, 0.01, and 1 sun under open circuit conditions. The recombination is bulk dominated with a minimum at the p/i interface, highlighted by the ovals, at low illumination intensities. The recombination shifts towards the p/i interface with increasing illumination intensity, where it is clearly dominant at 1 sun. Such an increase in recombination at the p/i interface is also observed in the dark J_D-V characteristics when the forward bias is increased. When the dark J_D-V and light J_{sc}-V_{oc} characteristics are combined, superposition of the experimental results is observed (Fig. 21a) which is consistent with the simulation (Fig. 21b). By combining such dark J_D-V and light J_{sc}-V_{oc} characteristics, valuable information is obtained about the mechanisms limiting the V_{oc} and its stability.

If J_{sc}-V_{oc} characteristics superimpose over the bulk-dominated J_D-V characteristics, as discussed in the next section on superposition, it is possible to determine the contributions of the bulk – albeit not necessarily at 1 sun. The contributions of the bulk can be observed in both J_{sc}-V_{oc} and dark J_D-V characteristics with a constant diode quality factor (slope) at low bias. Extrapolation of this slope in the J_{sc}-V_{oc} characteristic to 1 sun illumination is an indication of the bulk limitation to the 1 sun V_{oc}. However, this is not the ultimate limit of the V_{oc} for a given a-Si:H material because changes in the p layer, which result in changes in the built-in potential,

affect the field dependent recombination in the bulk. The insensitivity of the results found here using different high quality p-layers indicate that V_{bi} is not a limiting factor for V_{oc}, and furthermore that its effect on the recombination is not of first order.

Finally, it should be noted that the proceeding discussion is further complicated owing to the inhomogeneous and evolutionary nature of optimum a-Si:H growth (i.e., protocrystallinity). When both the microstructure and electronic properties of the i layer are changing with thickness – bulk properties are ephemeral. In addition, the "substrate effect" (i.e., the fact that the phase, microstructure, and electronic properties of the p and i-layers depend on the substrate on which they are deposited) leads to complications in assigning absolute values of the bandgap and the density of states for the p, p/i interface, and i layers. This additional complexity makes it very difficult to alter one variable at a time in experimental studies. For example, the introduction of a material with a different microstructure at the p/i interface layer during p-i-n solar cell growth affects the properties of the subsequent i-layer. This particular scenario can be surmounted using the n-i-p structures that are currently under investigation.

C. The Superposition Principle

In addition to the diagnostic value that the dark J-V characteristics provide, they also allow, in certain circumstances, the prediction of solar cell parameters under different illumination levels via the superposition principle. The superposition principle, based on an equivalent circuit analysis, states that if a system is linear, its response to several simultaneous excitations is simply the sum of the response to each individual excitation applied alone. Generally speaking, the current in an illuminated solar cell (J_L) is described by the dark J-V characteristic (J_D) shifted by the measured short circuit current (J_{sc}), which can be represented by the equation: $J_L(V) = J_D(V) - J_{sc}$ Although the a-Si:H p-i-n diode cannot be described as a linear

system and the photocurrent is highly dependent upon the applied bias, several comments can be made about the V_{oc}. In fact, the V_{oc} of a solar cell is determined by a balance between the light-generated J and the opposing forward bias diode J. The presence of a relationship between diode dark currents and the photogenerated currents under open-circuit conditions is well established for crystalline solar cells. Although in general there is no simple analytical expression for V_{oc}, it can be described by the superposition-based relation: $J_{sc} - J_D(V_{oc}) = 0$, since at V_{oc} $J_L(V)=0$. If the superposition principle is valid, then the measured V_{oc} would satisfy the above equation, and a plot of J_{sc} versus V_{oc} measured over a range of illumination intensities would superimpose on the dark J-V characteristics for the same diode. Deviations from this can, however, occur at high forward biases and corresponding illumination intensities. In this regime, the current are not dominated by the recombination in thin regions at the p/i interface in the presence of highly non-uniform distributions of carriers. The difference in obtaining carrier densities between injection and generation by light and subsequent extraction has to be taken into account. Uncertainty about the nature of the p/i interface at this time does not allow such effects to be quantified.

Despite the many experimental results and theoretical calculations disproving its validity, several workers[8,9] have reported the presence of the superposition principle in a-Si:H based solar cells. It is shown here that for high quality cells, whose carrier recombination currents are determined by the bulk, the superposition is valid under open-circuit conditions over extended regions of J_D-V and J_{sc}-V_{oc}. This can be seen in Fig. 21 which depicts experimental results and calculations for an a-Si:H p-i-n cell having a 4000Å thick R=10 i-layer. The results obtained for J_D-V and J_{sc}-V_{oc} obtained over a wide range of illumination intensities coincide over a range of bias voltages.

[8] S. Hegedus, N. Salzman and E. Fagan, *J. Appl.Phys*. **63**, 5126 (1998).
[9] A. Madan and T.J. McMahon, *Mat. Res. Soc. Symp. Proc*. **49**, 287 (1985).

Isolation of the cells by etching the n-layer back to the i-layer in the p-i-n cells minimizes shunt currents and permits accurate measurements at low voltages and intensities.

Theoretical studies on solar cells have proposed that the superposition principle can be applied to devices wherein both the dark currents and the photogenerated currents are dominated by recombination in a depletion region similar to the case of a-Si:H based solar cells[10]. The absence of superposition reported by many researchers and the ongoing debate over whether or not it is valid in a-Si:H based diodes is probably due to the highly defective i-layer materials and/or poor cell structure designs used in such work. The lack of superposition in an a-Si:H p-i-n cell with highly defective i-layers can be demonstrated by applying the continuity principle to the device analysis. In some of these studies, electroluminescence experiments of such diodes indicate that i-layer recombination is not dominant; however, in these devices recombination in the p-layer was determined to be the dominant transport mechanism. Very large quality factors of the diodes (n>2) indicate that these i-layers are of very low quality (i.e., defect density well above 10^{17} cm^{-3}) also leading to cells lacking in superposition. In most of these studies, the J-V characteristics were not extended to low voltages due to the presence of shunts.

In its most general form, the continuity principle states that in steady state the current flowing through the terminals of a solar cell must equal the difference between the total rate of photogeneration and the total rate of recombination in the device. This can be expressed by:

$$J_L(V) = q\int_{cell} G(x)dx - q\int_{cell} U(x)dx$$

where G(x) is the volume rate of photogeneration and U(x) is the volume rate of recombination.

[10] N.G. Tarr and D.L. Pulfrey, *IEEE Trans. Elec. Dev*. **ED-27**, 771 (1980).

Since $J_L(V)=0$ under open circuit conditions, this indicates that the principle of superposition will strictly hold only if the integral involving U for an illuminated cell differs from the same integral for a non-illuminated cell by at most a constant that does not depend on voltage. Modeling has been performed that accurately describes the cell whose superposition characteristics are shown in Fig. 21. In this modeling, it is found that for open-circuit conditions over a wide range of illumination intensities the quasi-Fermi levels across the i-layer are not appreciably displaced from their positions in the dark under a forward bias corresponding to that of the V_{oc}.

This is a direct consequence of the strong similarity in the carrier recombination kinetics present under open-circuit conditions for a given open-circuit voltage, V_{oc}, and the same forward bias voltage in the dark. This is illustrated in Fig. 22 where simulation results are shown for the cell in Fig. 21 using a density of 10^{16} cm^{-3} for the midgap states. Figure 22 (a) shows the quasi-Fermi level positions (F_n and F_p) and Fig. 22 (b) shows the carrier recombination profiles for the cell obtained under 10^{-3} sun illumination, which results in a V_{oc} of 0.70 V, as well as in the dark with the corresponding forward bias voltage of 0.70 V. Such a voltage is in the well-defined exponential region of the J-V characteristics illustrated in Fig. 21, where there is a clear overlap between the dark current density and that obtained under illumination.

In the case considered here, where the bulk densities of defects are on the order of 10^{16} cm^{-3}, the maximum recombination under 1 sun illumination occurs in the vicinity of the p/i interface. A strong similarity is observed between both the quasi-Fermi level positions and the carrier recombination profiles (and most importantly in the p/i interface region) as is illustrated in Fig. 22. It is important to note that such results are for a D^o density of 10^{16} cm^{-3}, which corresponds to the annealed state of the cell. Similar results are also found for the cell in the degraded steady state when D^o densities are ~$10^{17}cm^{-3}$; however, this is no longer true when the

density of these defects is increased to 10^{18} cm^{-3}, as illustrated with the simulations in Fig. 23. It can be seen in Fig. 23 (a) that the quasi-Fermi levels across the i-layer at V_{oc}, 0.55 V in this case, are significantly shifted from their positions when the same forward bias dark voltage is applied. This is also reflected in the difference between the recombination profiles in the dark and under illumination as shown in Fig. 23 (b). In contrast to the results shown in Fig. 22 (b), the maximum recombination rate under illumination at V_{oc} is about two orders of magnitude larger than that present in the dark at the same forward bias voltage. This clearly indicates that in cells with such large densities of defects superposition is no longer valid. In this case for $V_{oc}=V_f$, the J_{sc}-V_{oc} characteristic is shifted to much higher current densities compared to those obtained for the dark J-V.

It can be concluded from the above results and discussion that the a-Si:H based solar cells studied in this work having high quality i-layers, optimized p/i interfaces, and low midgap densities of states can be reliably characterized using a bulk recombination model. Furthermore their dark J-V characteristics coincide with the plots of the J_{sc}-V_{oc} pairs, indicating that the superposition principle applies under open-circuit conditions. This means that under these conditions, the carrier transport with and without illumination is very similar.

As a consequence it appears that dark current voltage characteristics can be used to obtain information about the transport and recombination of carriers relevant to solar cell performance. Providing the contributions of bulk and interface recombination to these characteristics can be clearly identified valuable information can be obtained about both. The characterization of well controlled p/i interface regions will offer new insights into the nature of the p/i interfaces and their effects on inputs for simulations which will allow for more reliable modeling than at present.

The voltage regimes clearly identified with bulk recombination on the other hand offer a tool for characterizing the gap states in the intrinsic layers. The information obtained from such studies in conjunction with those on corresponding thin films will greatly enhance the ability to characterize the nature , densities, and energy distribution of the intrinsic gap states as well as those created by SWE.

Figures

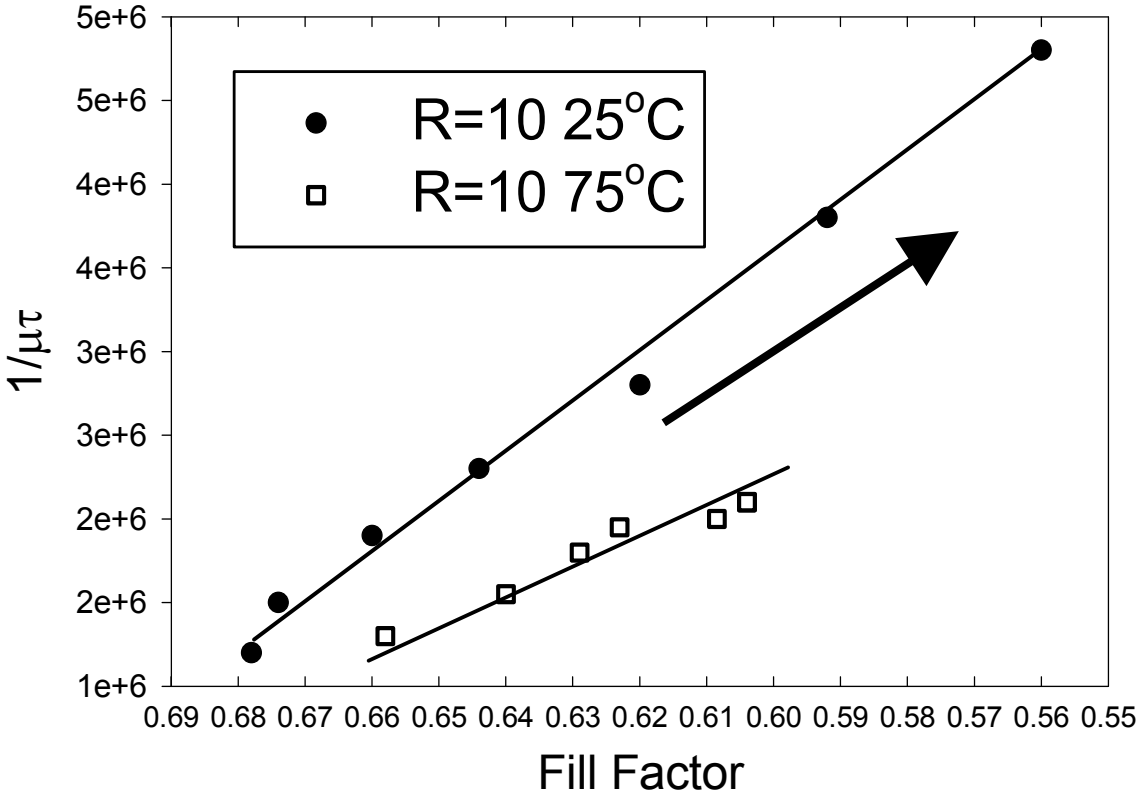

Fig. 1 FF vs. 1/μτ shown for a 7000Å p-i-n cell having an i-layer prepared under the same conditions as the corresponding film. Direction of arrow indicates increasing 1 sun illumination exposure time.

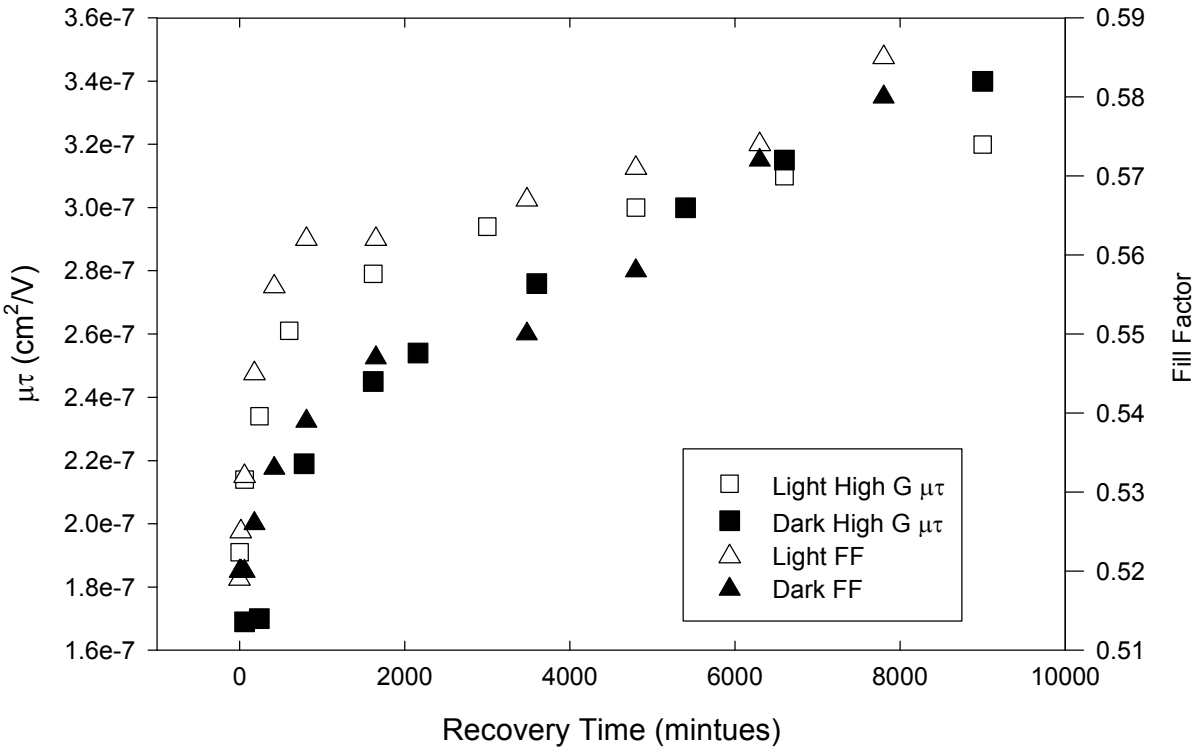

Fig. 2 Annealing kinetics of R=10 film (μτ) and solar cell (FF) from 10 sun degraded steady state in both the light and dark at 50°C.

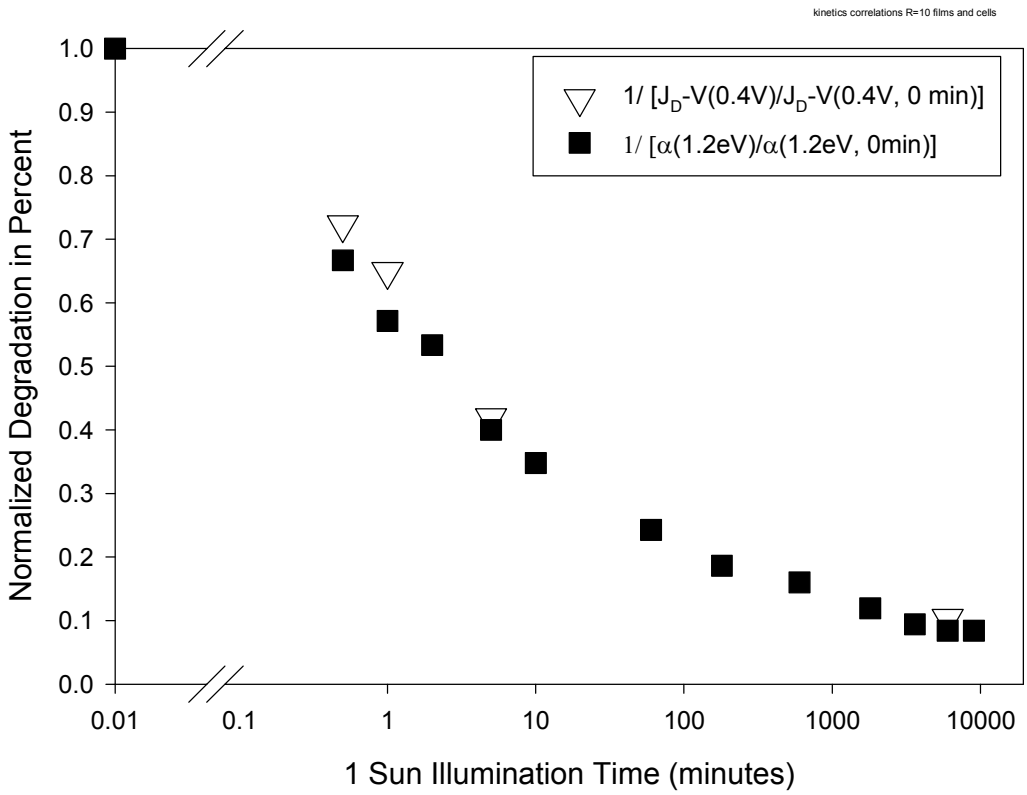

Fig. 3 Normalized degradation in percent under 1 sun illumination for J_D-V characteristics at 0.4 V for a p-i-n solar cell with an R=10 i layer; also shown is the corresponding increase in the α(E) characteristic at 1.2 eV for the i layer thin film.

Series	T_s (°C)	P (W/cm^2)	$R=[H_2]:[SiH_4]$ (sccm: sccm)		p_{tot} (Torr)	p_{silane} (Torr)	Dep. rate (nm/s)
A	200	0.08	0 = 0:5	(min)	0.07	0.07	0.12
			40 = 200:5	(max)	0.90	0.03	0.02
B	200	**0.83**	0 = 0:5	(min)	0.07	0.07	0.79
			40 = 200:5	(max)	0.90	0.03	0.20
C	**260**	**0.83**	0 = 0:5	(min)	0.07	0.07	0.77
			20 = 100:5	(max)	0.50	0.03	0.28
D	200	**0.34**	10 = 100:10	(min)	**4.00**	0.3	0.79
			100 = 200:2	(max)		0.01	0.21

Table I Summary of deposition conditions. For each series the minimum and maximum hydrogen-to-silane gas flow ratios $R=[H_2]/[SiH_4]$ are shown, along with the corresponding total and silane partial pressures and the measured deposition rates. Note that for series **D** the total pressure is kept constant, as opposed to the other three series for which the silane partial pressure is kept relatively constant at (0.05+/-0.02) Torr. The entries in bold are values differing from those of the standard series **A**.

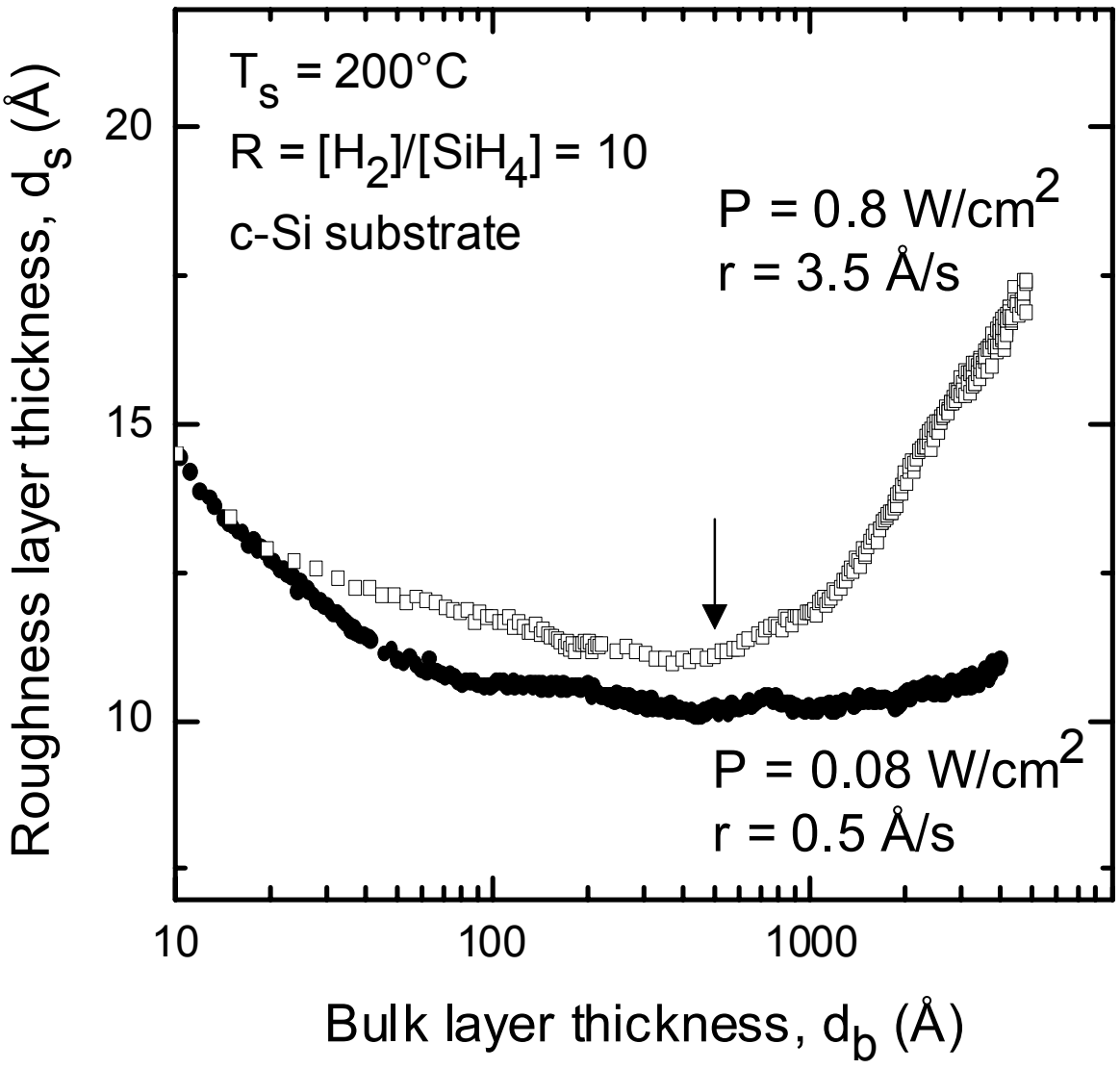

Fig. 4 Surface roughness layer thickness d_s as a function of bulk layer thickness d_b for a-Si:H films prepared on native-oxide-covered c-Si with fixed T=200°C and R=10, but different rf power levels of P=0.08 W/cm^2 (series **A** – filled circles) and 0.8 W/cm^2 (series **B** – open squares). For the higher P film, an amorphous-to-amorphous surface roughening transition (a→a) occurs near d_b=500 Å (arrow), whereas for the lower P film, any such transition must occur for d_b>4000 Å.

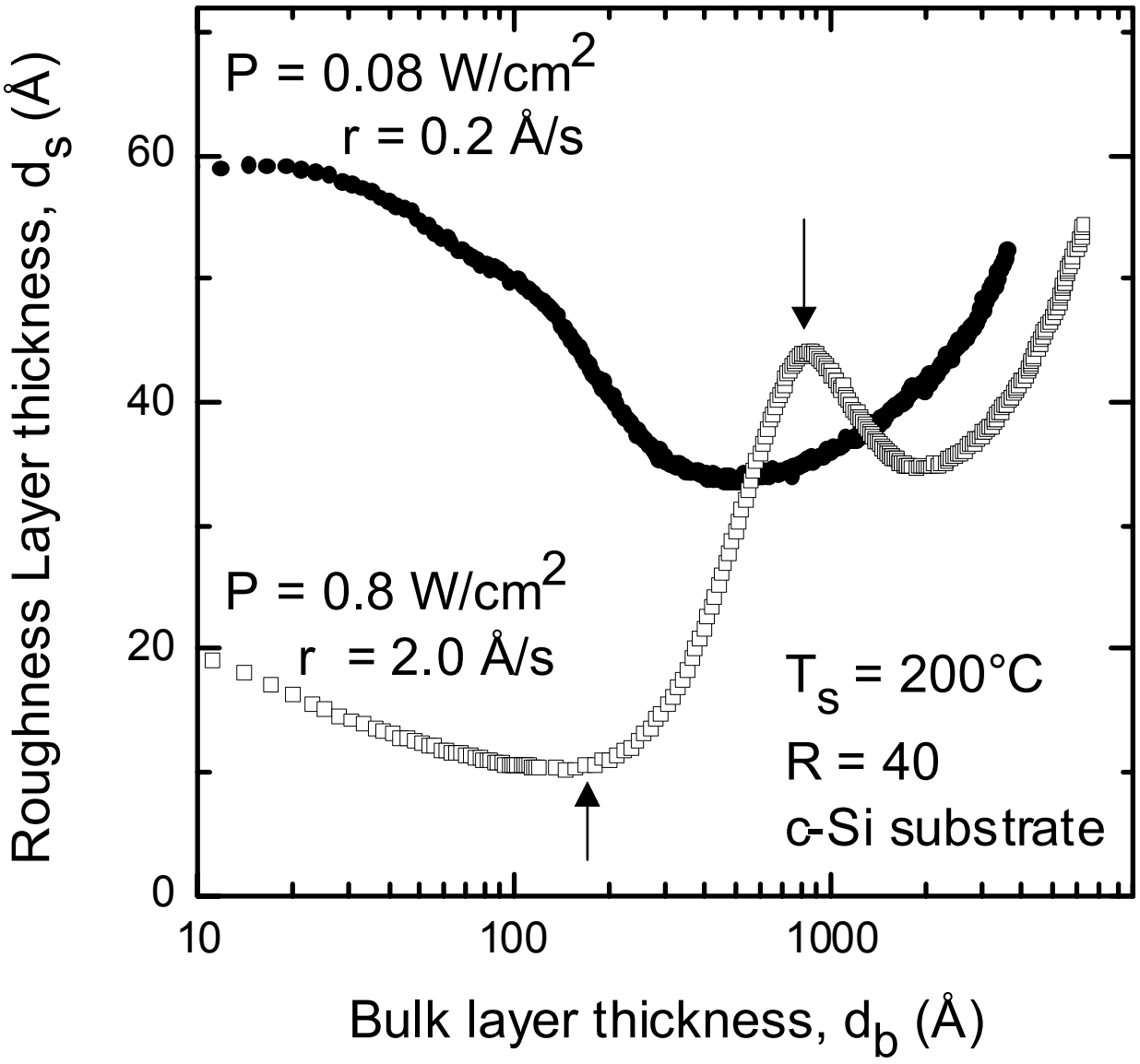

Fig. 5 Surface roughness layer thickness d_S as a function of bulk layer thickness d_b for Si:H films prepared on native-oxide-covered c-Si with fixed T=200°C and R=40, but different rf power levels of P=0.08 W/cm^2 (series **A** – filled circles) and 0.8 W/cm^2 (series **B** – open squares). For the lower P film, μc-Si:H nucleates immediately from the substrate, whereas for the higher P film, an amorphous–to–(mixed-phase-microcrystalline) transition [a→(a+ μc)] occurs near d_b=170 Å.

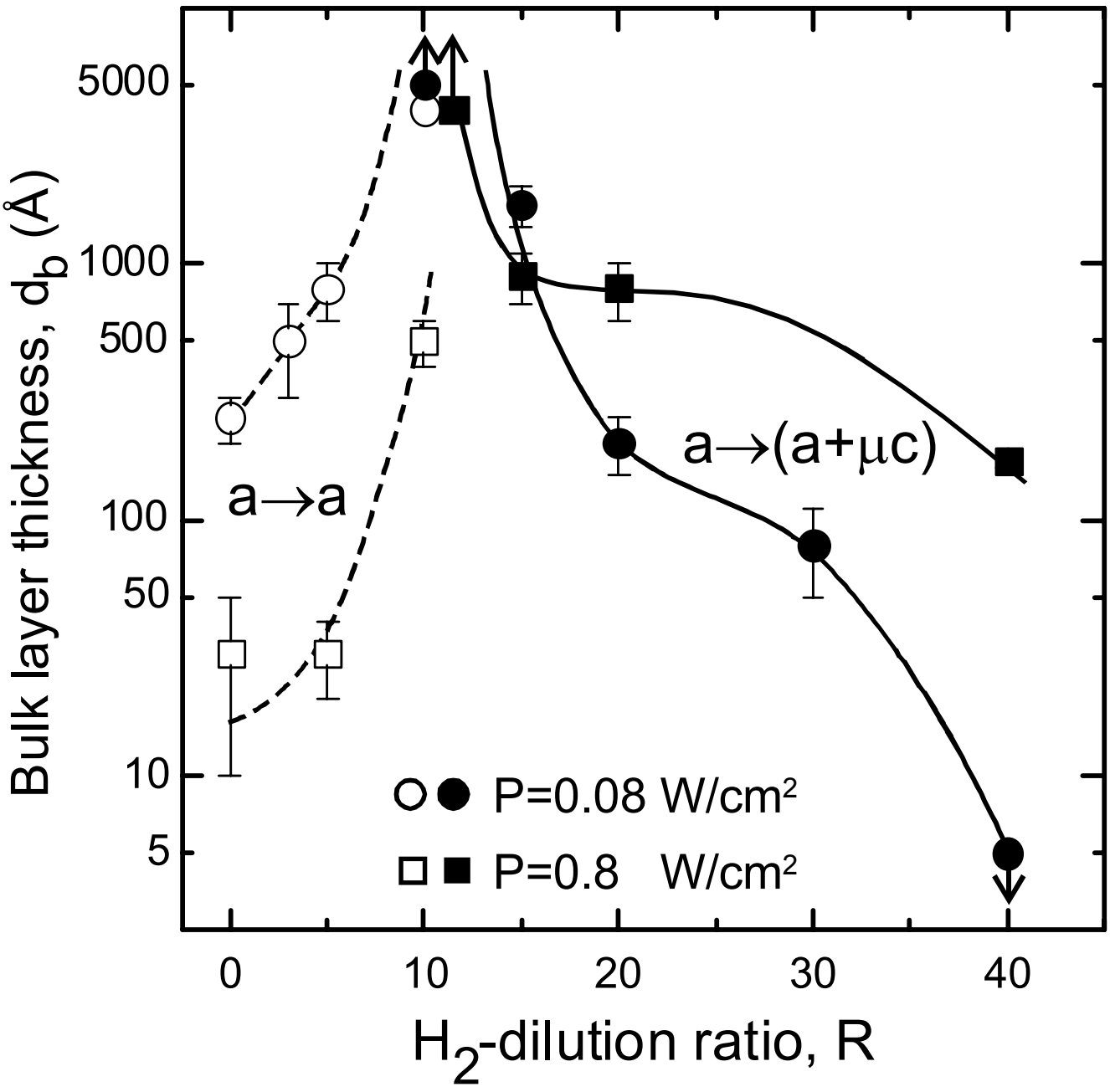

Fig. 6 Comparison between the phase diagrams for Si:H film deposition on c-Si at 200°C and two different rf powers: 0.08 W/cm^2 (series **A** - circles) and 0.8 W/cm^2 (series **B** - squares). The open symbols and broken lines indicate amorphous-to-amorphous roughening transitions [a→a], and the filled symbols and solid lines indicate amorphous-to-(mixed-phase-microcrystalline) [a→(a+μc)] transitions. The (up, down) arrows indicate that the transitions occur (above, below) the indicated thicknesses.

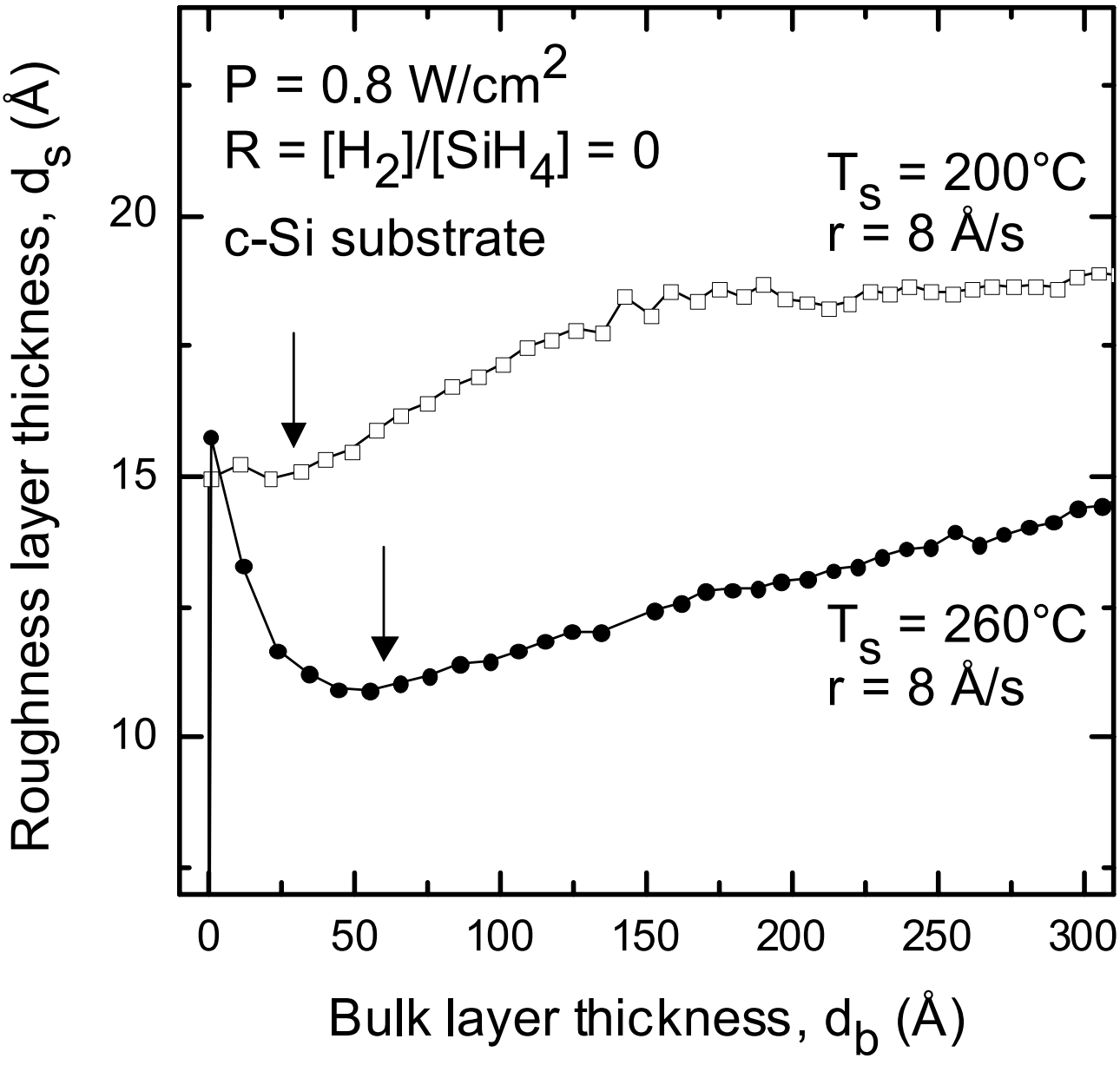

Fig. 7 Surface roughness layer thickness d_S vs. bulk layer thickness d_b for a-Si:H films prepared on native-oxide-covered c-Si with fixed R=0 and P=0.8 W/cm^2, but different substrate temperatures of T=200°C (series **B** - open squares) and 260°C (series **C** - filled circles). For the T=200°C film, amorphous phase surface roughening begins immediately, whereas for the T=260°C film, the a→a roughening transition occurs near d_b=60 Å.

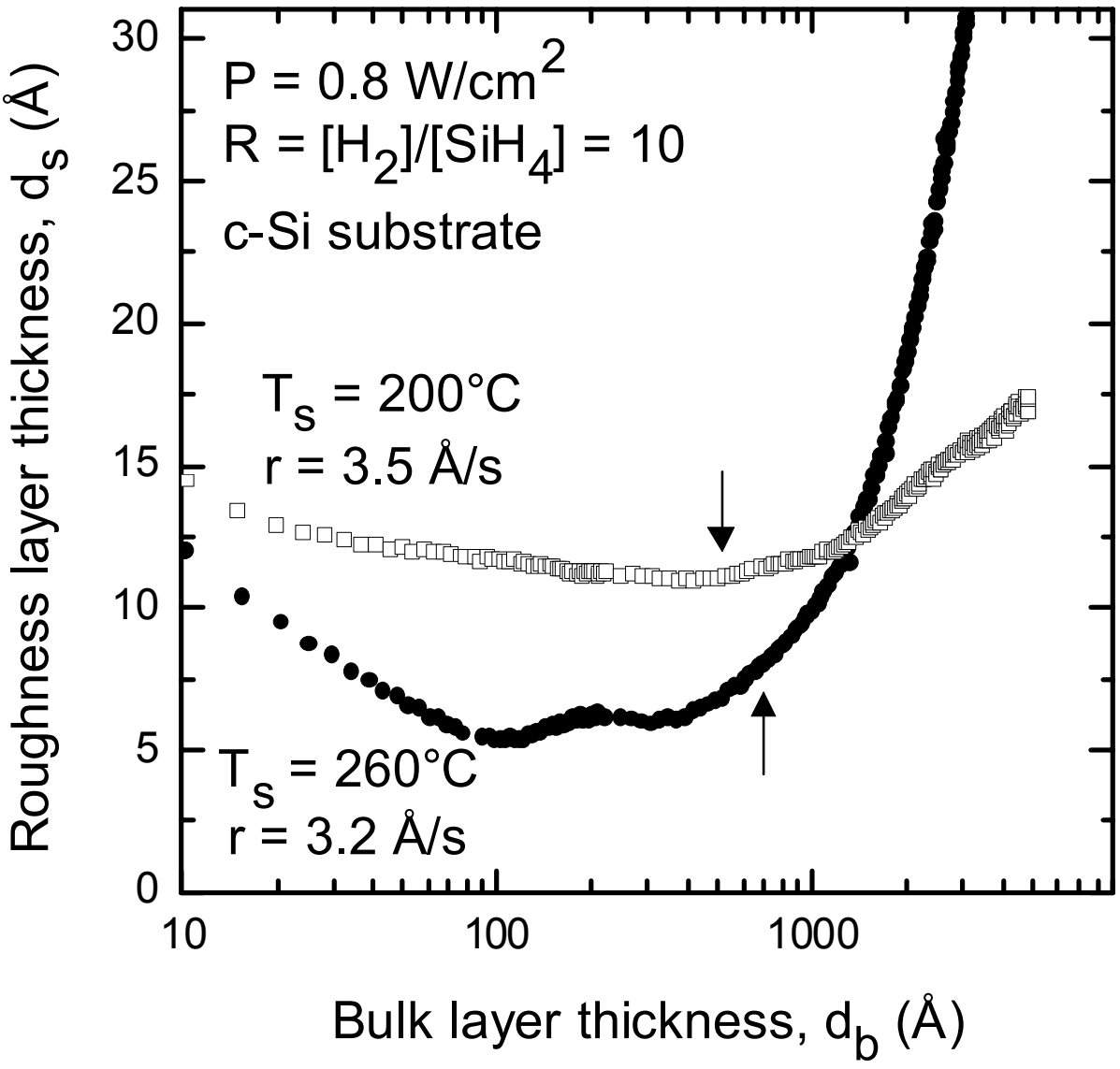

Fig. 8 Surface roughness layer thickness d_s vs. bulk layer thickness d_b for Si:H films prepared on native-oxide-covered c-Si with fixed R=10 and P=0.8 W/cm^2, but different substrate temperatures of T=200°C (series **B** - open squares) and 260°C (series **C** - filled circles). For the T=200°C film, the a$\rightarrow$a roughening transition occurs near d_b=500 Å, whereas for the T=260°C film, the a$\rightarrow$(a+μc) roughening transition occurs near d_b=700 Å.

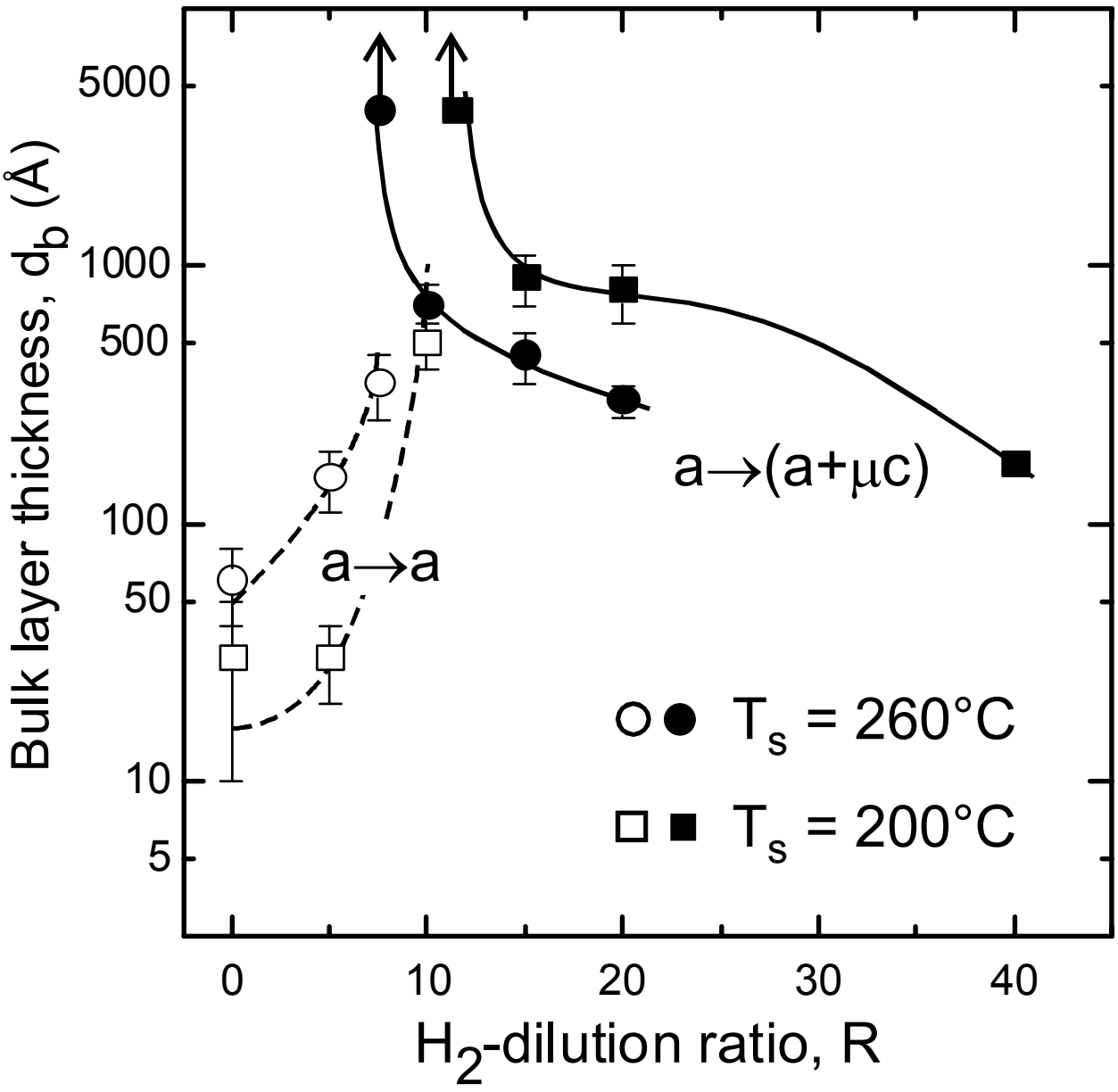

Fig. 9 Comparison between the phase diagrams for Si:H film deposition on c-Si at P=0.8 W/cm^2 and two different substrate temperatures: T=200°C (series **B** - squares) and 260°C (series **C** - circles). The open symbols and broken lines indicate the amorphous-to-amorphous roughening transitions [a→a], and the filled symbols and solid lines indicate the amorphous-to-(mixed-phase-microcrystalline) transitions [a→(a+μc)]. The up arrows indicate that the transition occurs above the indicated thicknesses.

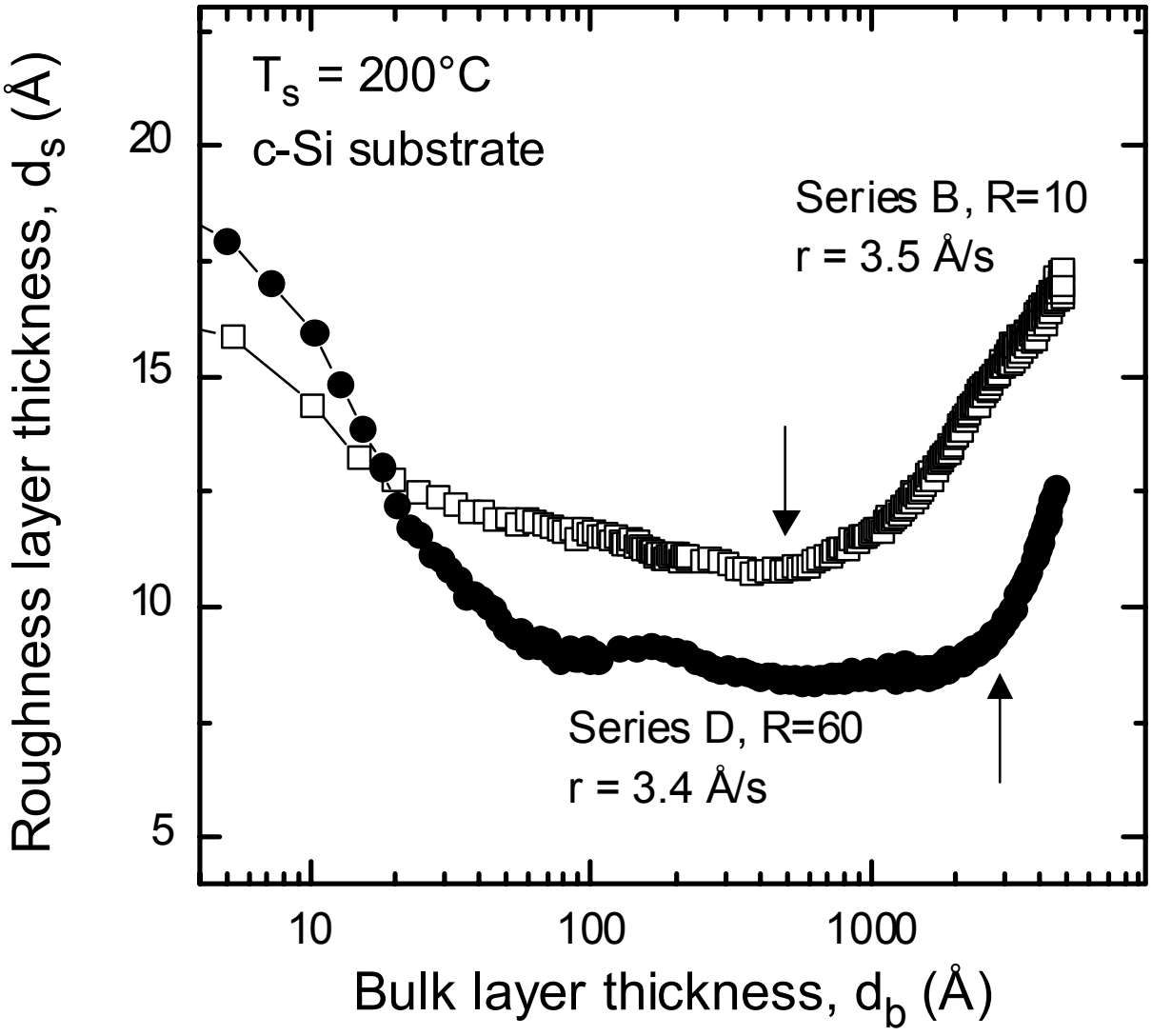

Fig. 10 Surface roughness layer thickness d_s vs. bulk layer thickness d_b for Si:H films prepared on native-oxide-covered c-Si from series **B** (open squares) and **D** (filled circles) with different total gas pressures of p_{tot}=0.4 and 4 Torr, respectively. For the p_{tot}=0.4 Torr deposition of series **B**, the rf plasma power was 0.8 W/cm^2 and the H_2 dilution ratio was R=10, yielding a rate of 3.5 Å/s. For the p_{tot}=4 Torr deposition of series **D**, the power was 0.3 W/cm^2 and the H_2 dilution ratio was R=60, yielding a similar rate of 3.4 Å/s. For the film with p_{tot}=0.4 Torr, the a→a roughening transition occurs near d_b=500 Å, whereas for the film with $p_{tot=4\ Torr}$, the a→(a+μc) roughening transition occurs near d_b=3000 Å.

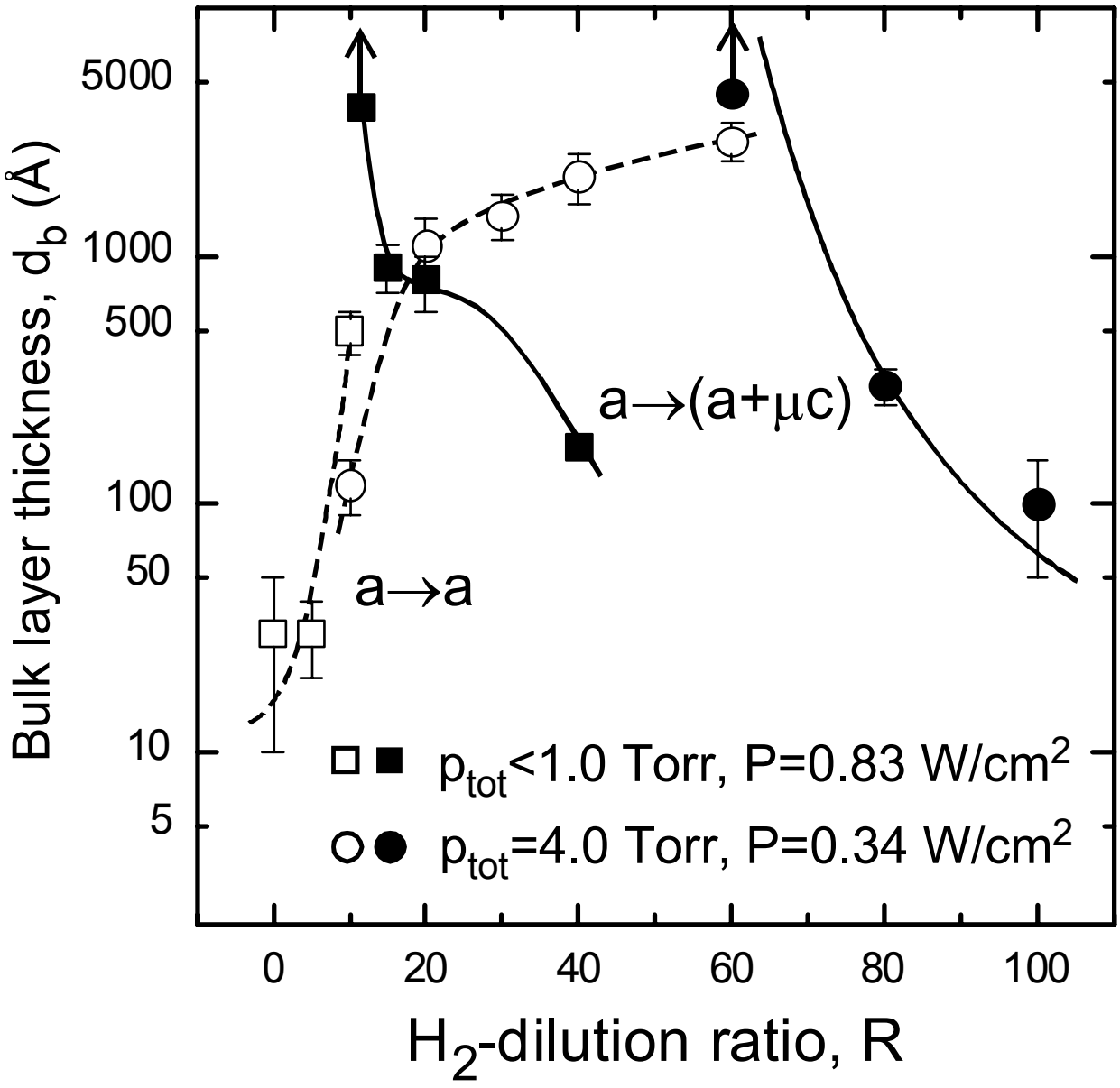

Fig. 11 Comparison between the phase diagrams for Si:H film deposition on c-Si for series **B** (squares) and series **D** (circles). The deposition parameters are P=0.8 W/cm^2 and p_{tot}<1 Torr for series **B**, and P=0.3 W/cm^2 and p_{tot}=4.0 Torr for series **D**. The open symbols and broken lines indicate the amorphous-to-amorphous roughening transitions [a→a], and the filled symbols and solid lines indicate the amorphous-to-(mixed-phase-microcrystalline) transitions [a→(a+μc)]. The up arrows indicate that the transition occurs above the indicated thicknesses.

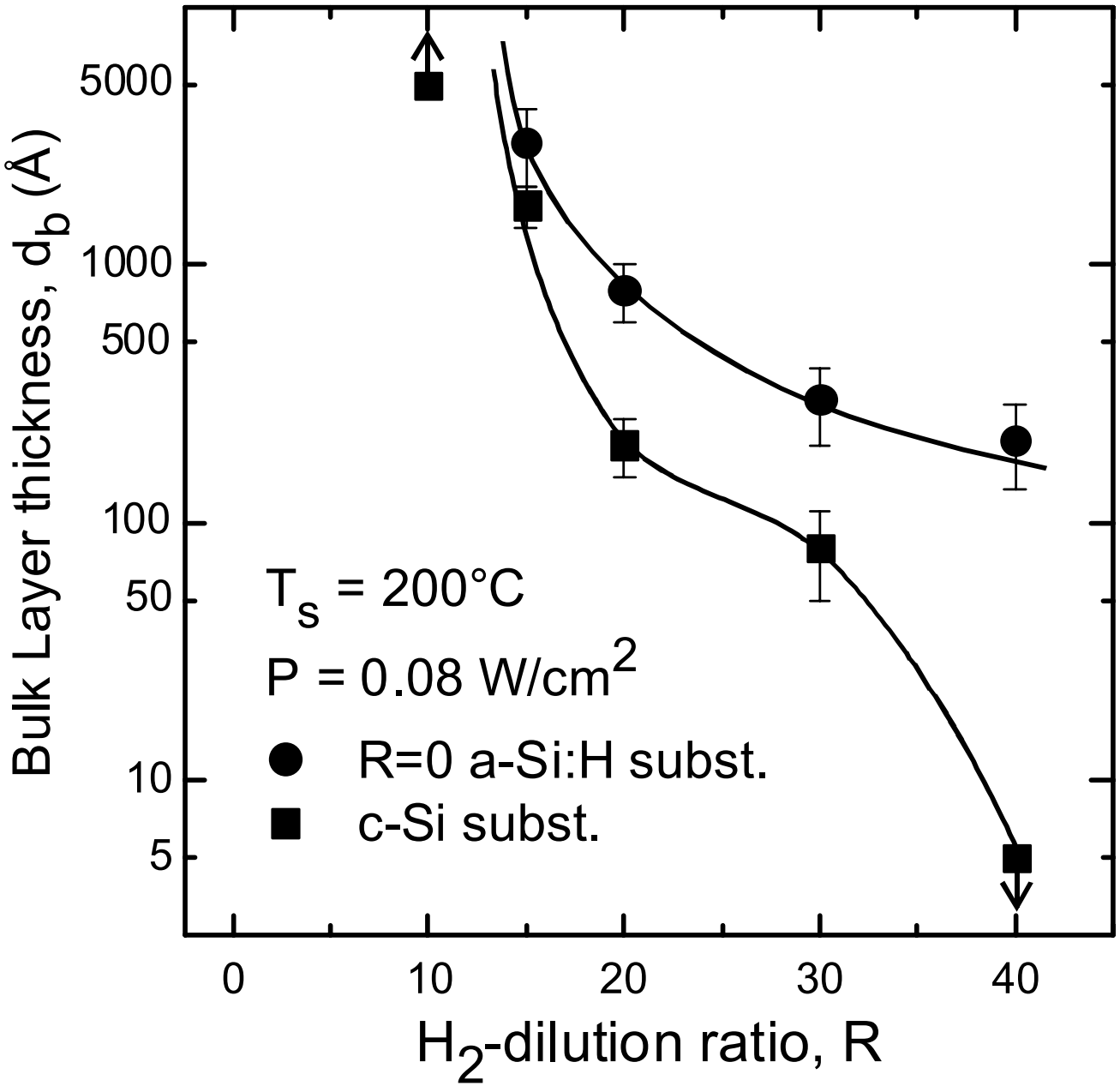

Fig. 12 Phase diagrams for Si:H film growth on native-oxide-covered c-Si (squares) and R=0 a-Si:H (circles) at T=200°C and P=0.08 W/cm^2. The solid lines indicate the amorphous−to−(mixed-phase-microcrystalline) transitions [a→(a+ μc)]. The (up, down) arrows indicate that the transition occurs (above, below) the indicated thicknesses.

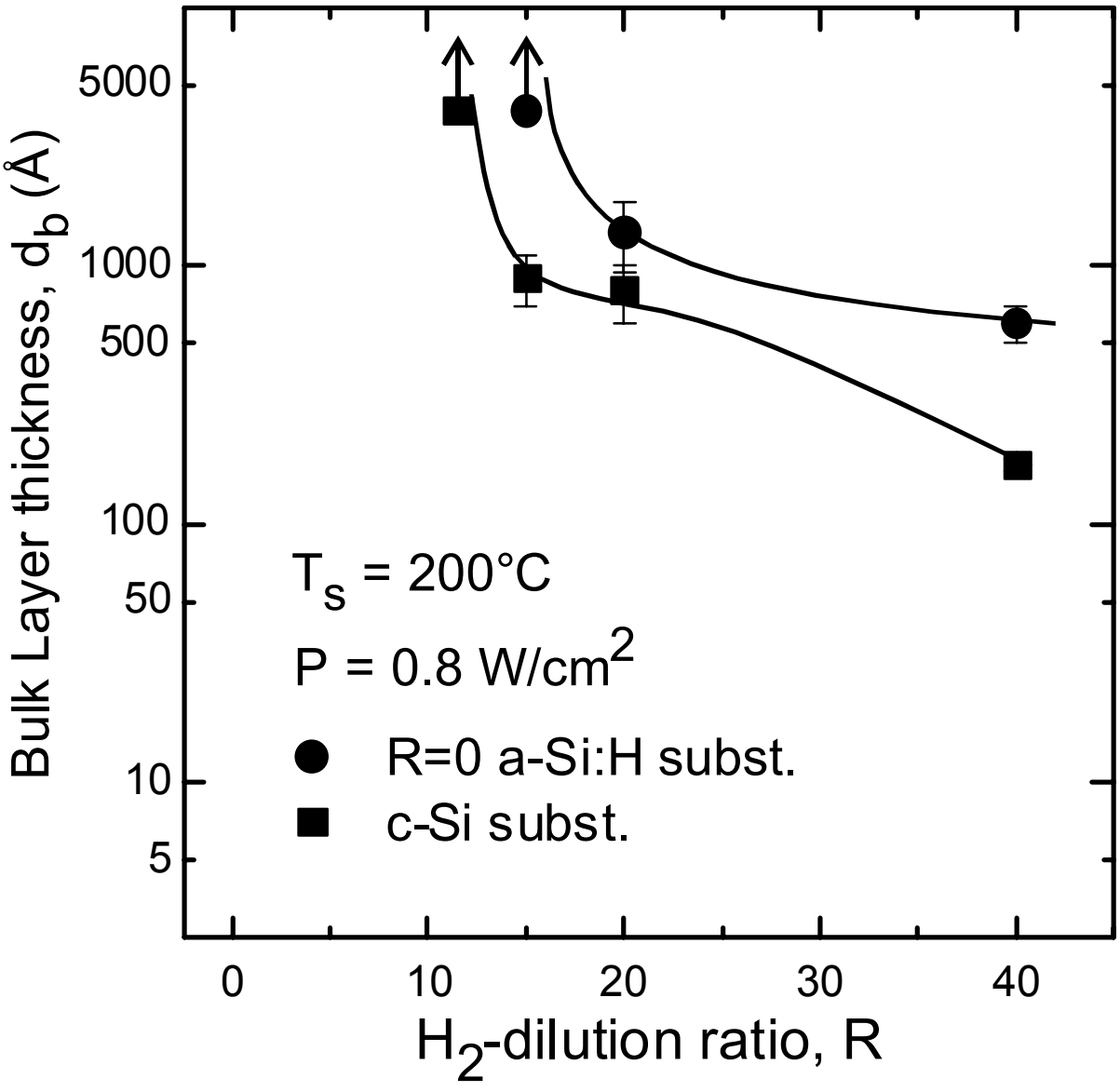

Fig. 13 Phase diagrams for Si:H film growth on native-oxide-covered c-Si (squares) and R=0 a-Si:H (circles) at T=200°C and P=0.8 W/cm^2. The solid lines indicate the amorphous–to–(mixed-phase-microcrystalline) transitions [a→(a+μc)]. The up arrows indicate that the transition occurs above the indicated thicknesses.

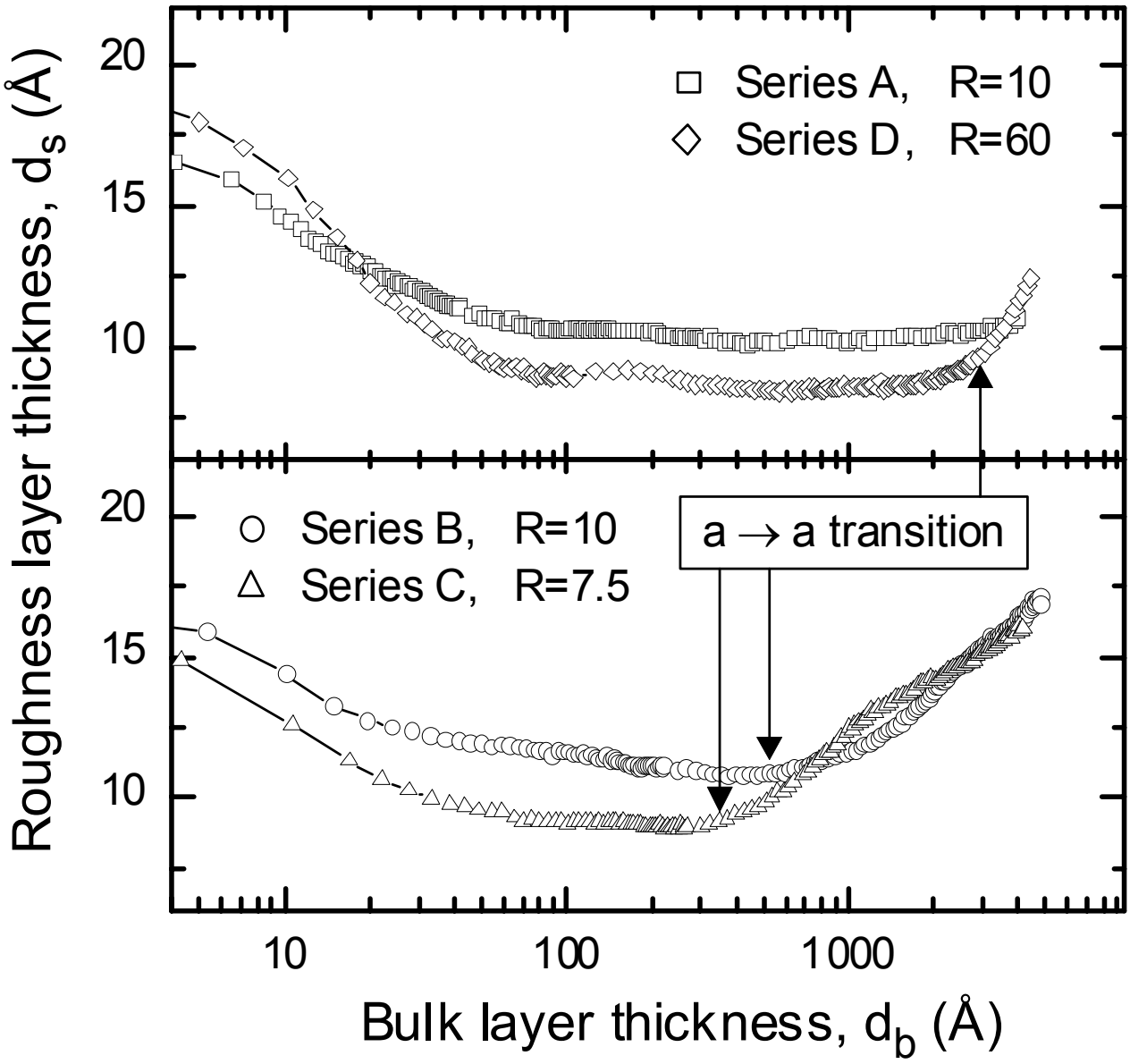

Fig. 14 Surface roughness layer thickness (d_S) evolution as a function of the bulk layer thickness (d_b) for one selected film of each series. The films were deposited under nominally "optimum condition" for each series, i.e., with maximum H_2-dilution possible without crossing the a→(a+μc) transition for a 300 nm a-Si:H film. The R value for each film is provided; other conditions are listed in Table I.

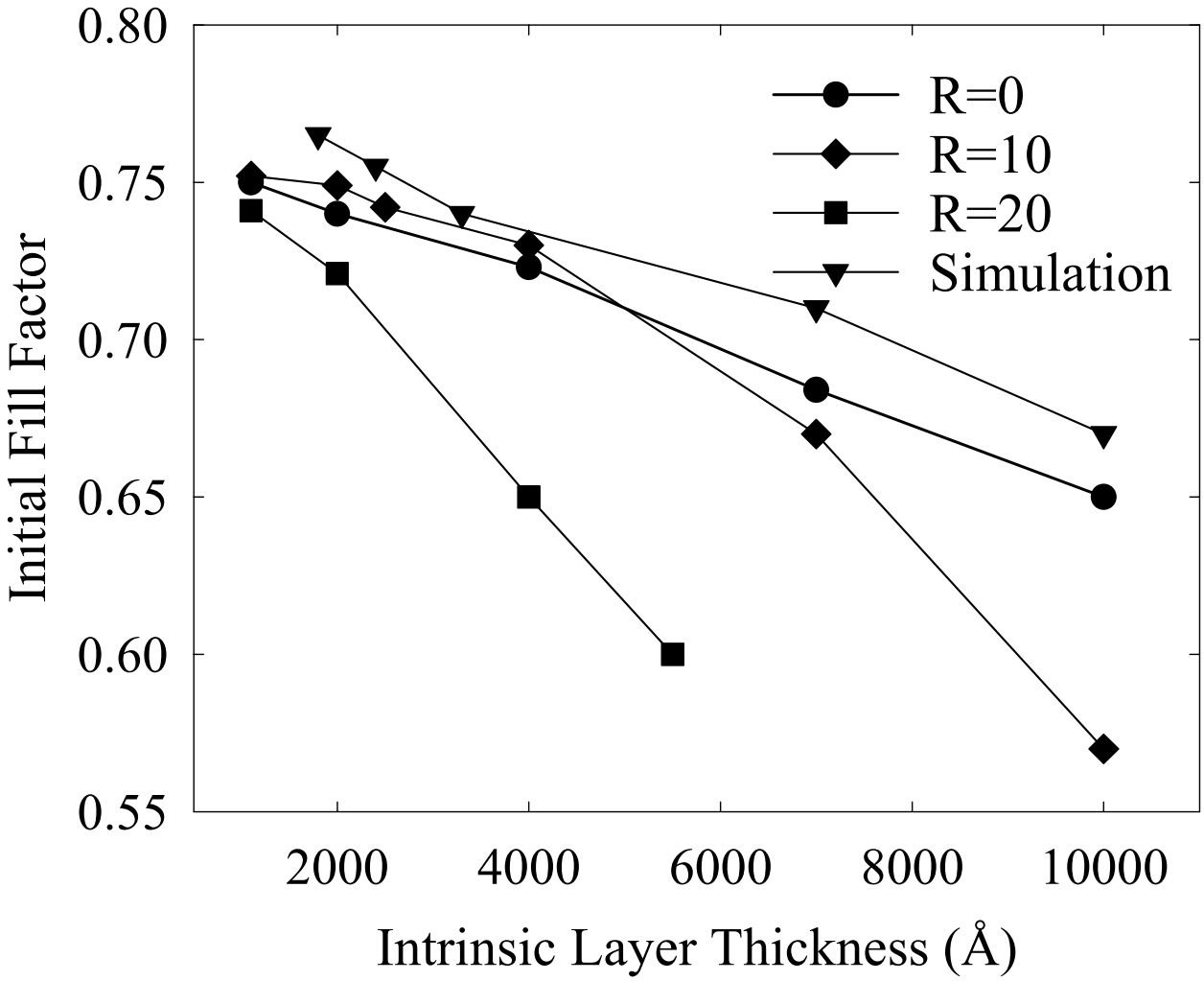

Fig. 15 Dependence of initial fill factor of p-i-n cells on the intrinsic layer thickness for R=0, 10, and 20. For comparison, simulation results for an R=0 structure having a homogeneous i-layer are also included.

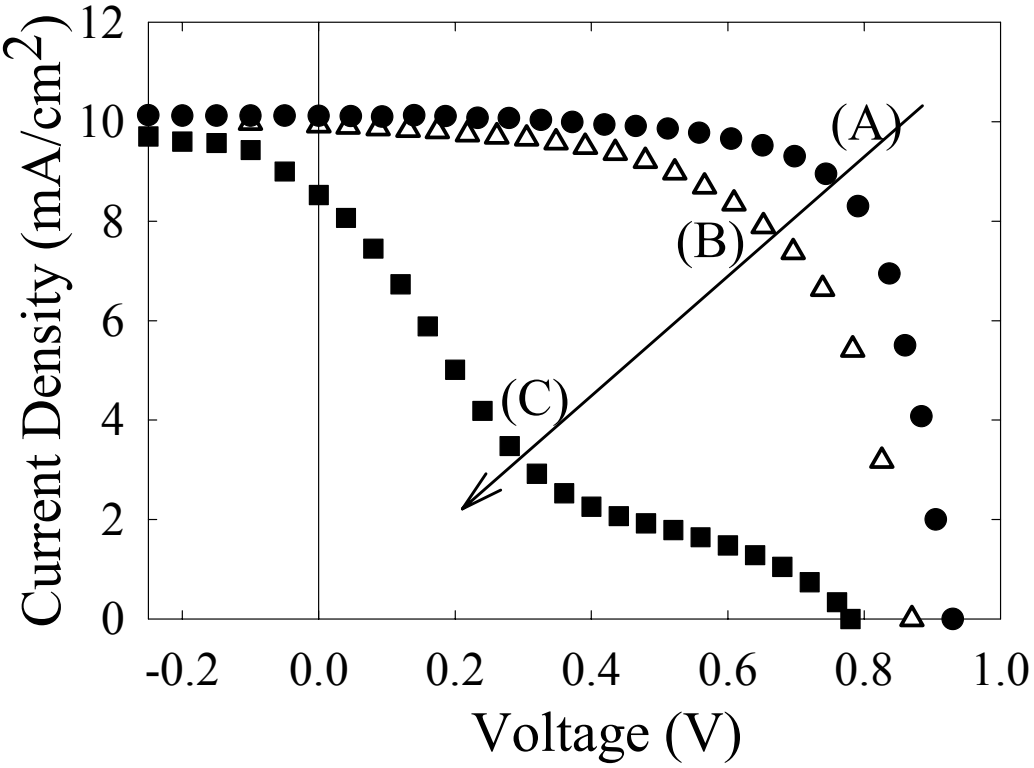

Fig. 16 J-V characteristics of cells A, B, and C measured at room temperature and under 1 sun illumination. Direction of arrow indicates decreasing distance between the p-contact and the a→(a+μc) transition.

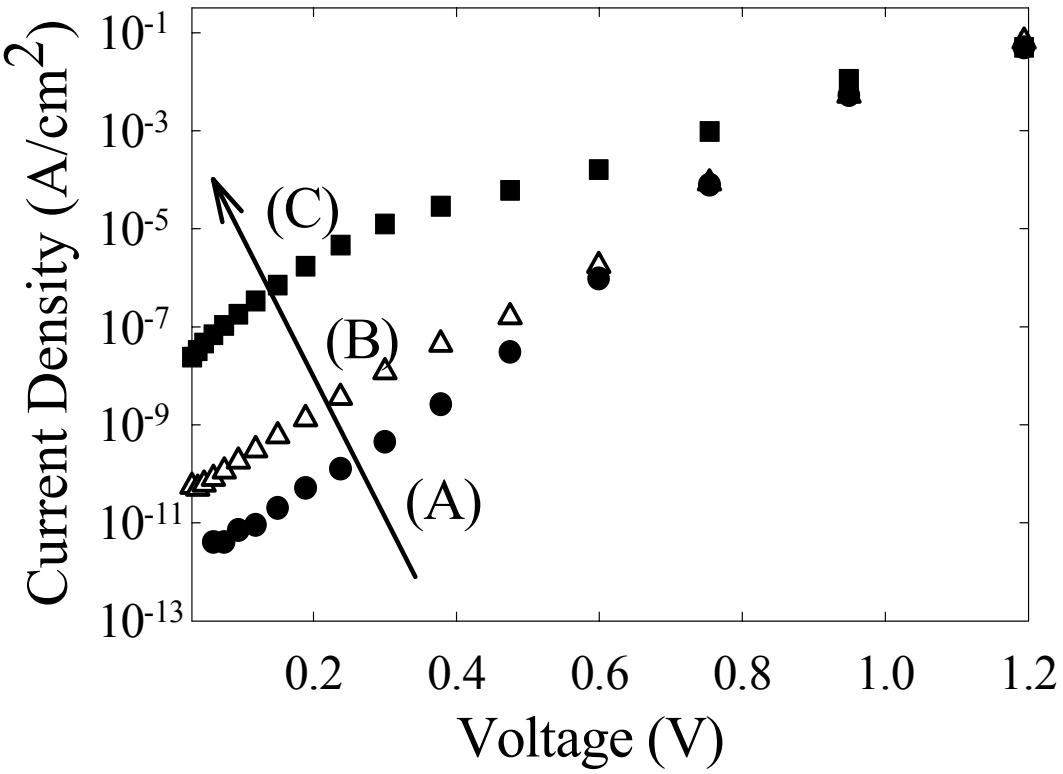

Fig. 17 J-V characteristics of cells A, B, and C measured at room temperature in the dark. Direction of arrow indicates decreasing distance between the p-contact and the a→(a+μc) transition.

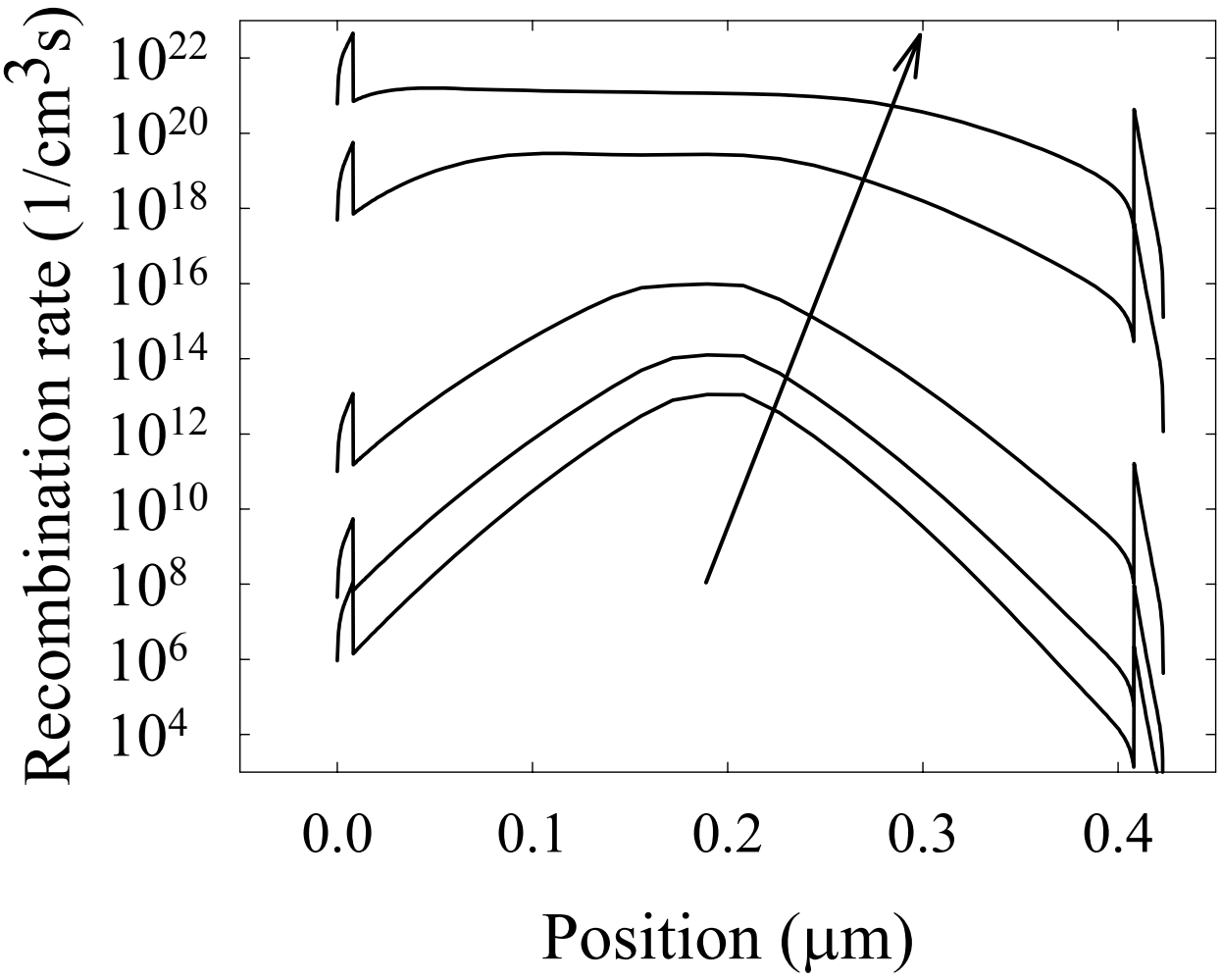

Fig. 18 Recombination profiles in the dark for a typical a-Si:H p-i-n solar cell having a homogeneous i-layer. Different values of forward bias voltage are shown (V=0.1, 0.2, 0.4, 0.8, 1.0 V) with the direction of the arrow indicating increasing forward bias voltage.

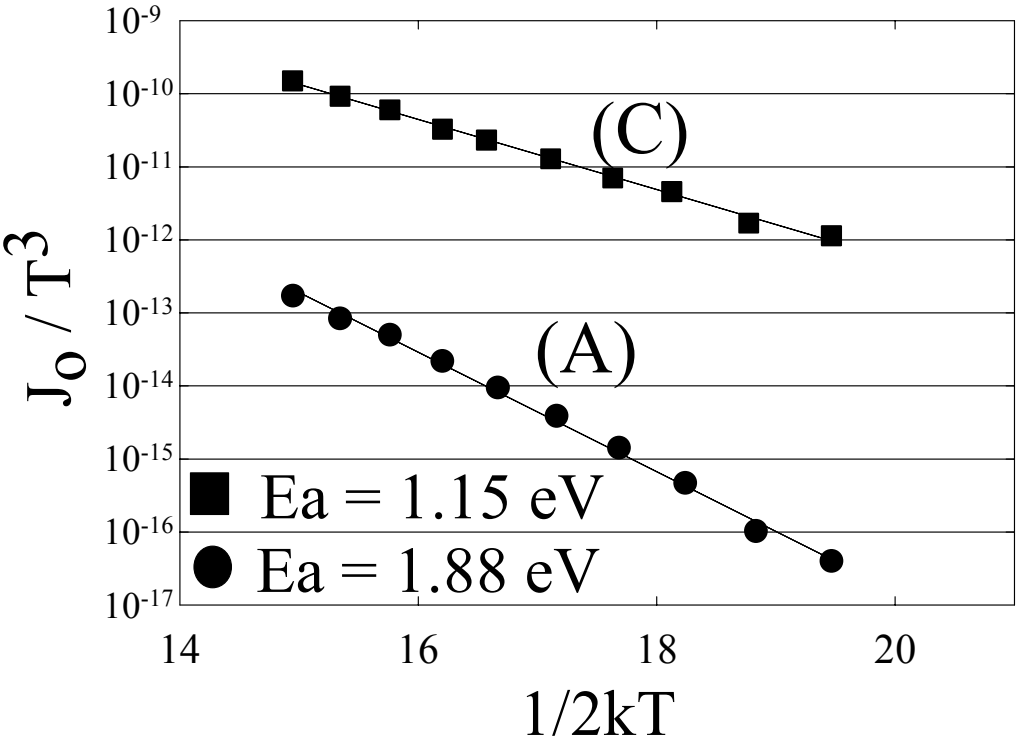

Fig. 19 Thermal activation plots of J_o/T^3 for the cells A and C. The symbols are experimental results and the solid lines are exponential fits used to extract the i-layer mobility gap.

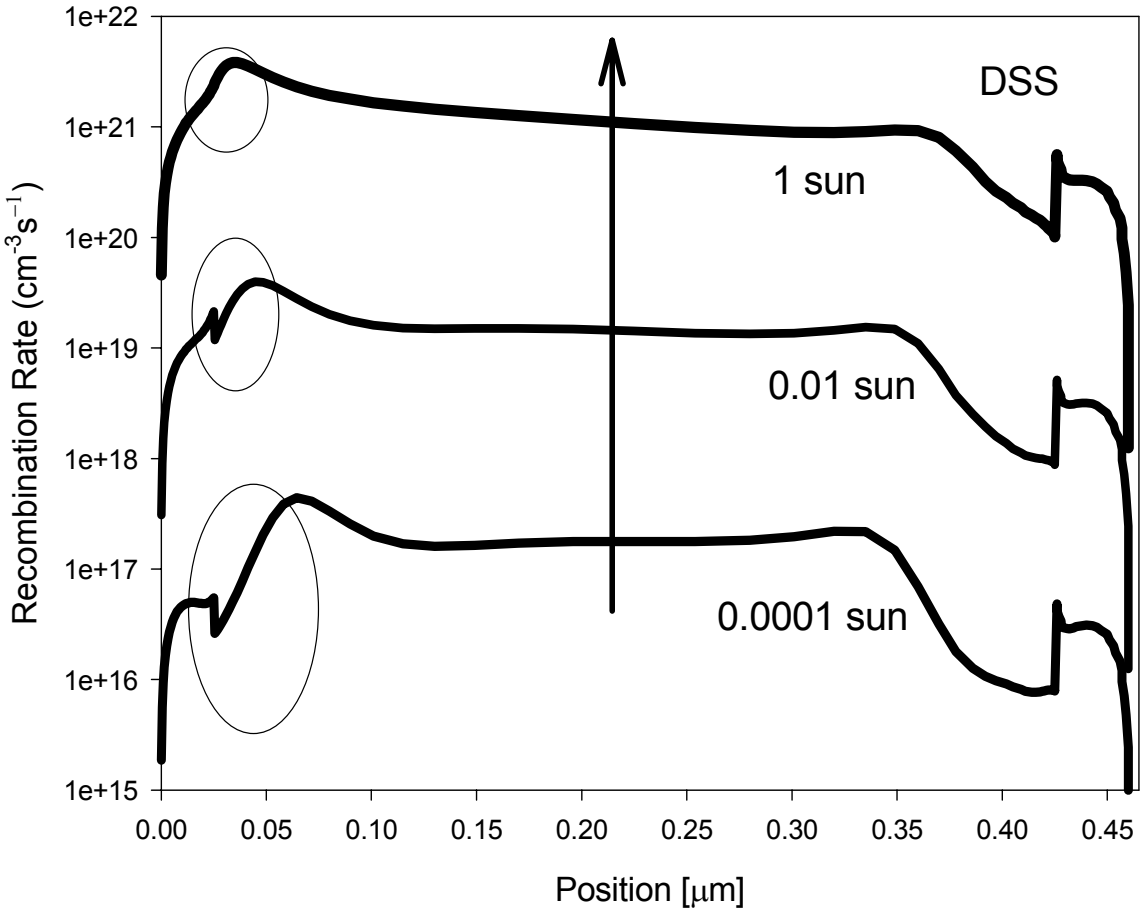

Fig. 20 AMPS simulation of recombination rates for an R=10 p-i-n solar cell in the degraded steady state at illumination intensities of 1, 0.01, and 0.0001 sun.

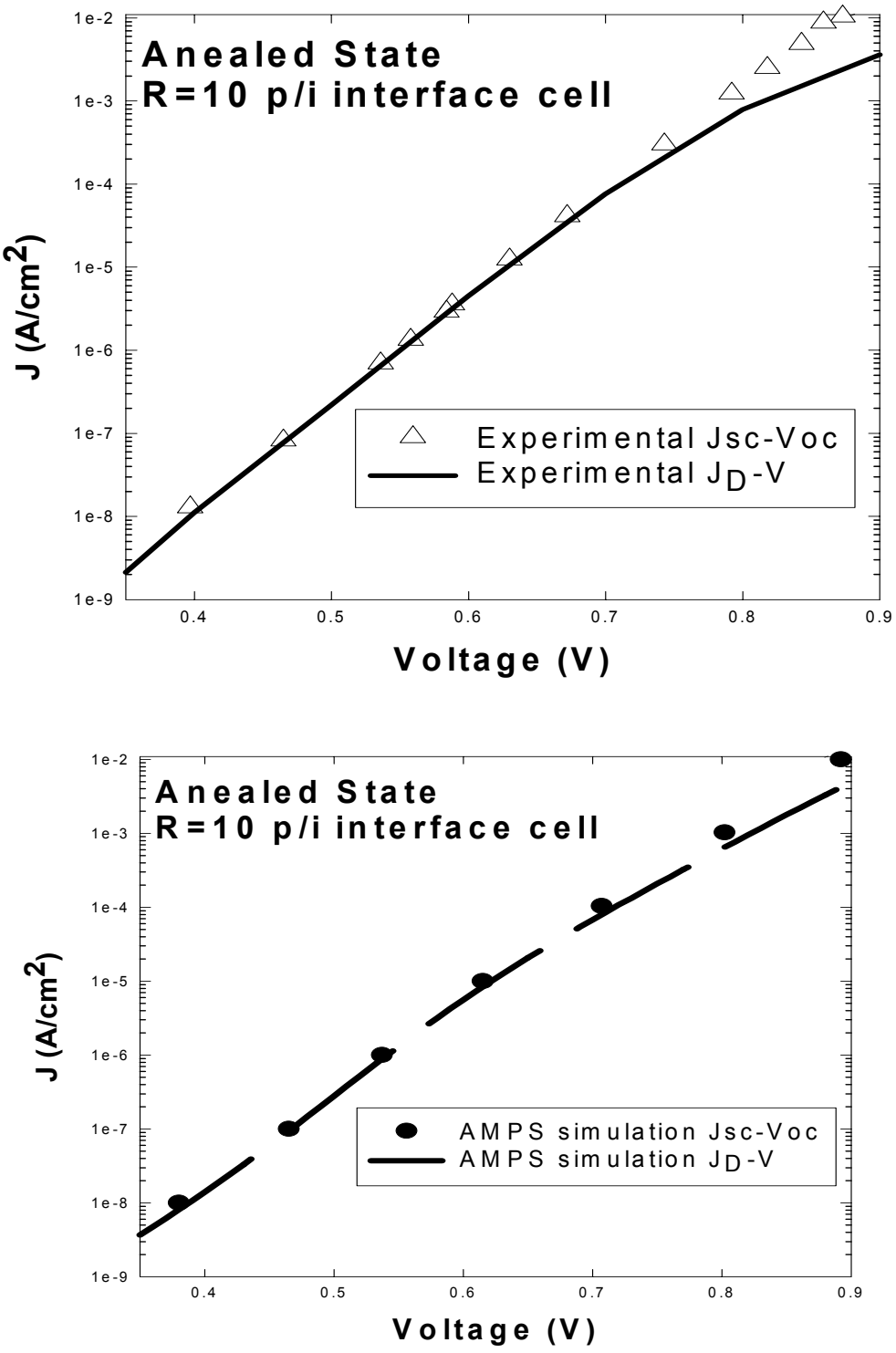

Fig. 21 (a) Dark J-V characteristics of an a-Si:H p-i-n solar cell having an i-layer prepared with R=10 to a thickness of 4000Å (solid line). Also shown are the J_{sc}-V_{oc} pairs for the same solar cell obtained over a wide range of illumination intensity (symbols). (b) AMPS simulation of the superposition of dark J-V and light J_{sc}-V_{oc} characteristics for an R=10 p-i-n solar cell.

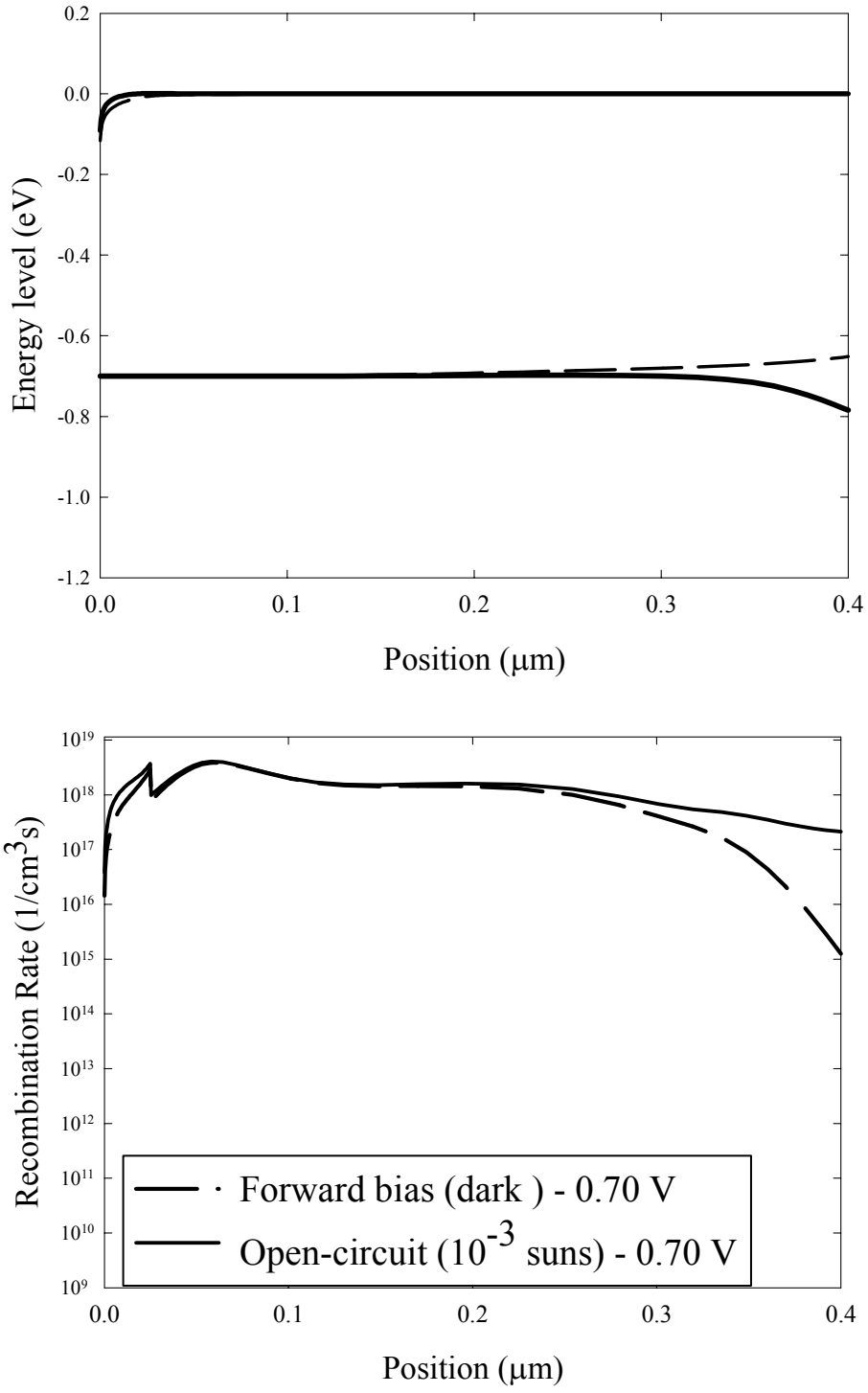

Fig. 22 (a) Simulation of electron and hole quasi-Fermi levels for an a-Si:H p-i-n solar cell obtained under 10^{-3} sun and open-circuit conditions (0.70 V) as well as in the dark under forward bias conditions (0.70 V). (b) Recombination profiles obtained under the same two sets of conditions. In both cases, $D^o=10^{16}$ cm^{-3}

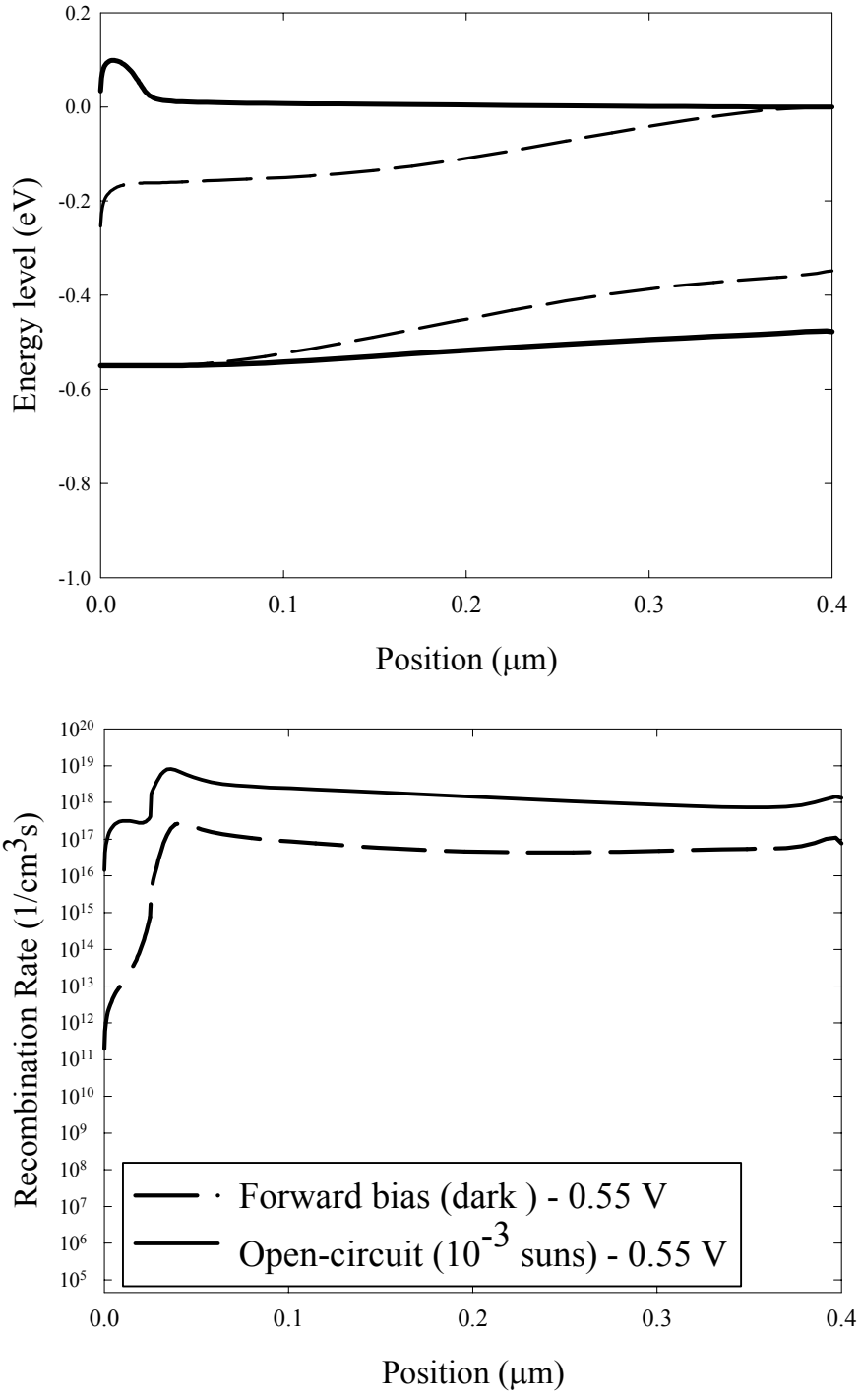

Fig. 23 (a) Simulation of electron and hole quasi-Fermi levels for an a-Si:H p-i-n solar cell obtained under 10^{-3} sun and open-circuit conditions (0.55 V) as well as in the dark under forward bias conditions (0.55 V). (b) Recombination profiles obtained under the same two sets of conditions. In both cases, $D^o=10^{18}$ cm^{-3}.

Appendices

Appendix A List of Collaborators

1. BP Solar

- Characterization of light induced degradation kinetics in protocrystalline Si:H cells at different deposition rates
- Mechanism for SWE
- Characterization of high rate r.f. PECVD a-Si:H cells
- Optical characterization of component materials of a-Si:H-based solar cells

2. United Solar Systems Corp.

- Characterization of light induced kinetics in protocrystalline Si:H materials and cells
- Establishing n-i-p (protocrystalline) cell capability at PSU comparable to that of (a-SiC:H)p-i-n cells
- Characterization of the microstructure of vhf high rate, low gap materials

3. National Renewable Energy Laboratory

- Characterization of light induced changes in hot-wire cells and materials
- Characterizing microstructure of hot-wire materials with SE
- Internal friction measurements of PSU a-Si:H materials
- Deriving self-consistent gap state distributions associated with SWE
- RTSE technology transfer

4. University of Toledo

- Optical characterization of intrinsic alloy materials for solar cells

Outside Collaborations:

ETL, Juelich, Eindhoven, Cracow, and KAIST

Appendix B: List of Publications

1. C. R. Wronski, invited talk, "Amorphous silicon photovoltaics: order from disorder", *IEEE Photovoltaic Specialists Conf. Proc.*, (IEEE, New York, 2000) pp. 1-6.

2. J. M. Pearce, R. J. Koval, R. W. Collins, and C. R. Wronski, "Quantitative correlation of high quality a-Si:H p-i-n solar cell characteristics with properties of the bulk and p/i interface region", *IEEE Photovoltaic Specialists Conf. Proc.*, (IEEE, New York, 2000) pp. 944-947.

3. R. J. Koval, J. M. Pearce, A. S. Ferlauto, P. I. Rovira, R. W. Collins, and C. R. Wronski, "The role of phase transitions in protocrystalline Si:H on the performance their of solar cells", *IEEE Photovoltaic Specialists Conf. Proc.,* (IEEE, New York, 2000) pp. 750-753.

4. A. S. Ferlauto, P. I. Rovira, R. J. Koval, C. R. Wronski, and R. W. Collins, "Effects of H_2-dilution and plasma power in amorphous silicon deposition: comparison of microstructural evolution and solar cell performance"*, IEEE Photovoltaic Specialists Conf. Proc.*, (IEEE, New York, 2000) pp. 713-716.

5. P. I. Rovira, A. S. Ferlauto, R. J. Koval, C. R. Wronski, and R. W. Collins, "Real time optics of p-type silicon deposition on specular and textured ZnO surfaces", *IEEE Photovoltaic Specialists Conf. Proc.*, (IEEE, New York, 2000) pp. 772-775.

6. C. R. Wronski, L. Jiao, R. J. Koval, and R. W. Collins, "Recent advances in understanding of a-Si:H based materials and performance of their solar cells", *Opto-Electron. Rev.* **8**, 275-279 (2000).

7. J. M. Pearce, R. J. Koval, A. S. Ferlauto, R. W. Collins, and C. R. Wronski, "Dependence of open-circuit voltage in hydrogenated protocrystalline silicon solar cells on carrier recombination in p/i interface and bulk regions", *Appl. Phys. Lett.* **77**, 3093-3095 (2000).

8. J. Lee, J. Koh, and R. W. Collins, "Multichannel Mueller matrix ellipsometer for real-time spectroscopy of anisotropic surfaces and films", *Opt. Lett.* **25**, 1573-1575 (2000).

9. J. A. Zapien, R. W. Collins, and R. Messier, "Multichannel ellipsometer for real time spectroscopy of thin film deposition from 1.5 to 6.5 eV", *Rev. Sci. Instrum.* **71**, 3451-3460 (2000).

10. J. M. Pearce, X. Niu, R. J. Koval, G. Ganguly, D. E. Carlson, R. W. Collins, and C. R. Wronski, "Contributions of D^O and non-D^O gap states to the kinetics of light induced degradation of amorphous silicon under 1 sun illumination", *Mater. Res. Soc. Symp. Proc.* **664**, A12.3.1-6 (2001).

11. R. J. Koval, J. M. Pearce, A. S. Ferlauto, R. W. Collins, and C. R. Wronski, "Evolution of the mobility gap with thickness in hydrogen-diluted intrinsic Si:H materials in the phase transition region and its effect on p-i-n solar cell characteristics", *Mater. Res. Soc. Symp. Proc.* **664**, A16.4.1-6 (2001).

12. A. S. Ferlauto, R. J. Koval, C. R. Wronski, and R. W. Collins, “Phase diagrams for the optimization of rf plasma-enhanced chemical vapor deposition of a-Si:H: variations in plasma power and substrate temperature”, *Mater. Res. Soc. Symp. Proc.* **664**, A5.4.1-6 (2001).

13. G. M. Ferreira, A. S. Ferlauto, P. I. Rovira, C. Chen, H. V. Nguyen, C. R. Wronski, and R. W. Collins, “Optical simulations of the effects of transparent conducting oxide interface layers on amorphous silicon solar cell performance”, *Mater. Res. Soc. Symp. Proc.* **664**, A24.6.1-6 (2001).

14. J. M. Pearce, R. J. Koval, A. S. Ferlauto, R. W. Collins, and C. R. Wronski, “Limitations of bulk generation-recombination on open circuit voltage under 1 sun illumination in amorphous silicon solar cells”, *Technical Digest of the 12th International Photovoltaic Science and Engineering Conference*, (2001) pp. 251-252.

15. C. R. Wronski, J. M. Pearce, R. J. Koval, and R. W. Collins, “Metastability in hydrogenated amorphous silicon based materials and solar cells”, *Technical Digest of the 12th International Photovoltaic Science and Engineering Conference*, (2001) pp. 33-36.

16. R. J. Koval, J. M. Pearce, A. S. Ferlauto, J. Koh, R. W. Collins, and C. R. Wronski, “Evolution of optoelectronic properties of hydrogen diluted Si:H materials and their effect on solar cell characteristics”, *Technical Digest of the Review Meeting for Research with Overseas Research Institutes*, (February 2, 2001) pp. 9-16.

17. R. W. Collins, A. S. Ferlauto, R. J. Koval, J. M. Pearce, P. I. Rovira, and C. R. Wronski, “Insights for improvement of silicon-based solar cells from real time optics studies”, *Technical Digest of the Review Meeting for Research with Overseas Research Institutes*, (February 2, 2001) pp. 1-8.

18. C. R. Wronski, R. J. Koval, J. M. Pearce, A. S. Ferlauto, J. Koh, and R. W. Collins, “Protocrystalline phase transitions in Si:H materials and their effect on solar cell characteristics”, *11th Workshop on Crystalline Silicon Cell Materials and Processes*, published as Rept. No. NREL/BK-520-30838, (August 19-22, 2001) pp. 93-94.

19. A. S. Ferlauto, G. M. Ferreira, C. Chen, P. I. Rovira, C. R. Wronski, R. W. Collins, X. Deng, and G. Ganguly, "Optical metrology for the next generation of a-Si:H-based thin film photovoltaics", in *Photovoltaics Beyond the 21st Century*, edited by R. McConnell and V. Kapur, (Electrochemical Society, Pennington NJ, 2001) Vol. 2001-10, pp. 199-228.

20. R. W. Collins, A. S. Ferlauto, R. J. Koval, J. M. Pearce, and C. R. Wronski, "Progress in high-stability amorphous silicon-based solar cells with guidance from real time optics", *Proceedings of the 2001 NCPV Review Meeting, 14-17 October 2001, Lakewood, Colorado*, (NREL, Golden CO, 2001), published as Rept. No. EL-520-31065, p. 21-22.

21. R. W. Collins, G. M. Ferreira, A. S. Ferlauto, C.Chen, C. R. Wronski, X. Deng, and G. Ganguly, "Progress in the optical measurement and modeling of multilayer thin film solar cell

structures", *Proceedings of the 2001 NCPV Review Meeting, 14-17 October 2001, Lakewood, Colorado*, (NREL, Golden CO, 2001), published as Rept. No. EL-520-31065, p. 173-174.

22. J. Lee, J. Koh, and R. W. Collins, "Dual rotating-compensator multichannel ellipsometer: instrument development for high-speed Mueller matrix spectroscopy of surfaces and thin films", *Rev. Sci. Instrum.* **72**, 1742-1754 (2001).

23. J. Lee, P. I. Rovira, I. An, and R. W. Collins, "Alignment and calibration of the MgF_2 biplate compensator for applications in rotating-compensator multichannel ellipsometry", *J. Opt. Soc. Am. A* **18**, 1980-1985 (2001).

24. A. S. Ferlauto, R. J. Koval, C. R. Wronski, and R. W. Collins, "Phase diagrams for Si:H film growth by plasma-enhanced chemical vapor deposition", *J. Non-Cryst. Solids*, (to be published, 2001).

25. R. J. Koval, J. M. Pearce, A. S. Ferlauto, R. W. Collins, and C. R. Wronski, "Mobility gap profiles in Si:H intrinsic layers prepared by H_2-dilution of SiH_4: effects on the performance of p-i-n solar cells", *J. Non-Cryst. Solids*, (to be published, 2001).

26. J. M. Pearce, R. J. Koval, X. Niu, S. J. May, R. W. Collins, and C. R. Wronski, "The 'fast' and 'slow' light induced defects in diluted and undiluted hydrogenated amorphous silicon solar cells and materials", *17th European Photovoltaic Solar Energy Conference Proceedings*, (to be published, 2001).

27. J. M. Pearce, R. J. Koval, A. S. Ferlauto, J. Koh, R. W. Collins, and C. R. Wronski, "Light induced changes in protocrystalline and amorphous silicon materials and their solar cells", *Mater. Res. Soc. Proc.* (submitted, 2002).

28. R. J. Koval, C. Chen, G. M. Ferreira, A. S. Ferlauto, J. M. Pearce, P. I. Rovira, C. R. Wronski, and R. W. Collins, "Protocrystalline Si:H p-type layers for maximization of the open circuit voltage of a-Si:H n-i-p solar cells", *Mater. Res. Soc. Proc.* (submitted, 2002).

29. C. R. Wronski, J. M. Pearce, R. J. Koval, A. S. Ferlauto, and R. W. Collins, "Progress in amorphous silicon-based solar cells", *Rio 2002 World Climate and Energy Event* (submitted, 2002).

30. A. S. Ferlauto, R. J. Koval, C. R. Wronski, and R. W. Collins, "Extended phase diagrams for guiding plasma-enhanced chemical vapor deposition of silicon thin films for photovoltaics applications", *Appl. Phys. Lett.* (submitted, 2002).

Appendix C: List of Presentations 2001

Review Meeting for Research with Overseas Research Institutes, Tokyo, Japan (February)

R. J. Koval, J. M. Pearce, A. S. Ferlauto, J. Koh, R. W. Collins, and C. R. Wronski, “Evolution of optoelectronic properties of hydrogen diluted Si:H materials and their effect on solar cell characteristics”.

R. W. Collins, A. S. Ferlauto, R. J. Koval, J. M. Pearce, P. I. Rovira, and C. R. Wronski, “Insights for improvement of silicon-based Solar cells from real time optics studies”.

Spring 2001 Materials Research Society Meeting, San Francisco CA, USA (April)

J. M. Pearce, X. Niu, R. J. Koval, G. Ganguly, D. E. Carlson, R. W. Collins, and C. R. Wronski, “Contributions of D^O and non-D^O gap states to the kinetics of light induced degradation of amorphous silicon under 1 sun illumination”.

R. J. Koval, J. M. Pearce, A. S. Ferlauto, R. W. Collins, and C. R. Wronski, “Evolution of the mobility gap with thickness in hydrogen-diluted intrinsic Si:H materials in the phase transition region and its effect on p-i-n solar cell characteristics”.

A. S. Ferlauto, R. J. Koval, C. R. Wronski, and R. W. Collins, "Phase diagrams for the optimization of rf plasma-enhanced chemical vapor deposition of a-Si:H: Variations in plasma power and substrate temperature".

G. M. Ferreira, A. S. Ferlauto, P. I. Rovira, C. Chen, H. V. Nguyen, C. R. Wronski, and R. W. Collins, "Optical simulations of the effects of transparent conducting oxide interface layers on amorphous silicon solar cell performance".

Electrochemical Society Meeting, Symposium on Photovoltaics Beyond the 21st Century, Washington DC, USA (May)

A. S. Ferlauto, G. M. Ferreira, C. Chen, P. I. Rovira, C. R. Wronski, R. W. Collins, X. Deng, and G. Ganguly, "Optical metrology for the next generation of a-Si:H-based thin film photovoltaics".

12th International Photovoltaic Science and Engineering Conference, Jeju, Korea (June)

J. M. Pearce, R. J. Koval, A. S. Ferlauto, R. W. Collins, and C. R. Wronski, “Limitations of bulk generation-recombination on open circuit voltage under 1 sun illumination in amorphous silicon solar cells”.

C. R. Wronski, J. M. Pearce, R. J. Koval, and R. W. Collins, “Metastability in hydrogenated amorphous silicon based materials and solar cells”.

19th International Conference on Amorphous & Microcrystalline Semiconductors Science & Technology, Nice, France (August)

A. S. Ferlauto, R. J. Koval, C. R. Wronski, and R. W. Collins, "Phase diagrams for Si:H film growth by plasma-enhanced chemical vapor deposition".

R. J. Koval, J. M. Pearce, A. S. Ferlauto, R. W. Collins, and C. R. Wronski, “ Mobility gap profiles in Si:H intrinsic layers prepared by H_2-dilution of SiH_4: effects on the performance of p-i-n solar cells”.

11th Workshop on Crystalline Silicon Cell Materials and Processes, Denver CO, USA (August)

C. R. Wronski, R. J. Koval, J. M. Pearce, A. S. Ferlauto, J. Koh, and R. W. Collins, “Protocrystalline phase transitions in Si:H materials and their effect on solar cell characteristics”.

17th European Photovoltaic Solar Energy Conference, Munich, Germany (October)

J. M. Pearce, R. J. Koval, X. Niu, S. J. May, R. W. Collins, and C. R. Wronski, “The ‘fast’ and ‘slow’ light induced defects in diluted and undiluted hydrogenated amorphous silicon solar cells and materials”.

National Center for Photovoltaics Program Review Meeting, Lakewood CO, USA (October)

R. W. Collins, A. S. Ferlauto, R. J. Koval, J. M. Pearce, and C. R. Wronski, "Progress in high-stability amorphous silicon-based solar cells with guidance from real time optics".

R. W. Collins, G. M. Ferreira, A. S. Ferlauto, C. Chen, C. R. Wronski, X. Deng, and G. Ganguly, "Progress in the optical measurement and modeling of multilayer thin film solar cell structures".

REPORT DOCUMENTATION PAGE

Form Approved
OMB NO. 0704-0188

1. AGENCY USE ONLY (Leave blank)	2. REPORT DATE	3. REPORT TYPE AND DATES COVERED
	July 2002	Final Report, 17 July 1998–16 November 2001

4. TITLE AND SUBTITLE
Stable a-Si:H-Based Multijunction Solar Cells with Guidance from Real-Time Optics, Final Report, 17 July 1998–16 November 2001

5. FUNDING NUMBERS
CF: XAF-8-17619-22
PVP25001

6. AUTHOR(S)
C.R. Wronski, R.W. Collins, J.M. Pearce, R.J. Koval, A.S. Ferlauto, G.M. Ferreira, and C. Chen

7. PERFORMING ORGANIZATION NAME(S) AND ADDRESS(ES)
Center for Thin Film Devices
Pennsylvania State University
University Park, PA 16802

8. PERFORMING ORGANIZATION REPORT NUMBER

9. SPONSORING/MONITORING AGENCY NAME(S) AND ADDRESS(ES)
National Renewable Energy Laboratory
1617 Cole Blvd.
Golden, CO 80401-3393

10. SPONSORING/MONITORING AGENCY REPORT NUMBER
NREL/SR-520-32692

11. SUPPLEMENTARY NOTES
NREL Technical Monitor: B. von Roedern

12a. DISTRIBUTION/AVAILABILITY STATEMENT
National Technical Information Service
U.S. Department of Commerce
5285 Port Royal Road
Springfield, VA 22161

12b. DISTRIBUTION CODE

13. ABSTRACT *(Maximum 200 words)*
This report describes the new insights obtained into the growth of hydrogenated silicon (Si:H) films via real-time spectroscopic ellipsometry (RTSE) measurements. Evolutionary phase diagrams were expanded to include the effects of different deposition conditions, including rf power, pressure, and temperature. Detailed studies of degradation kinetics in thin films and corresponding solar cells have been carried out. Both p-i-n and n-i-p solar cells that incorporate Si:H i-layers deposited with and without H_2-dilution have been studied. For the first time, direct and reliable correlations have been obtained between the light-induced changes in thin-film materials and the degradation of the corresponding solar cells.

14. SUBJECT TERMS: PV; real-time spectroscopic ellipsometry (RTSE); plasma-enhanced chemical vapor deposition (PECVD); amorphous silicon; degradation kinetics; high rate growth; sun illumination; mixed-phase-optimization microcrystalline materials; hydrogen dilution; real-time optics

15. NUMBER OF PAGES

16. PRICE CODE

17. SECURITY CLASSIFICATION OF REPORT	18. SECURITY CLASSIFICATION OF THIS PAGE	19. SECURITY CLASSIFICATION OF ABSTRACT	20. LIMITATION OF ABSTRACT
Unclassified	Unclassified	Unclassified	UL